Supporting Information: Exploring the origin of electron spin polarization in the metal-containing chromophore-radical system via multireference calculations

Ryosuke Sowa*,† and Yuki Kurashige*,†,‡,¶

†*Department of Chemistry, Graduate School of Science, Kyoto University, Kitashirakawa Oiwake-cho, Sakyo-ku Kyoto, 606-8502, Japan*

‡*FOREST, JST, Honcho 4-1-8, Kawaguchi, Saitama 332-0012, Japan*

¶*CREST, JST, Honcho 4-1-8, Kawaguchi, Saitama 332-0012, Japan*

E-mail: sowa@theoc.kuchem.kyoto-u.ac.jp; kura@kuchem.kyoto-u.ac.jp

1 Optimized structures of each molecule in the ground state

In this section, we present the optimized ground-state structures of molecules. The molecular structures were visualized using the VESTA software.[S1]

1.1 bpy-Pt-CAT-*m*Ph-NN

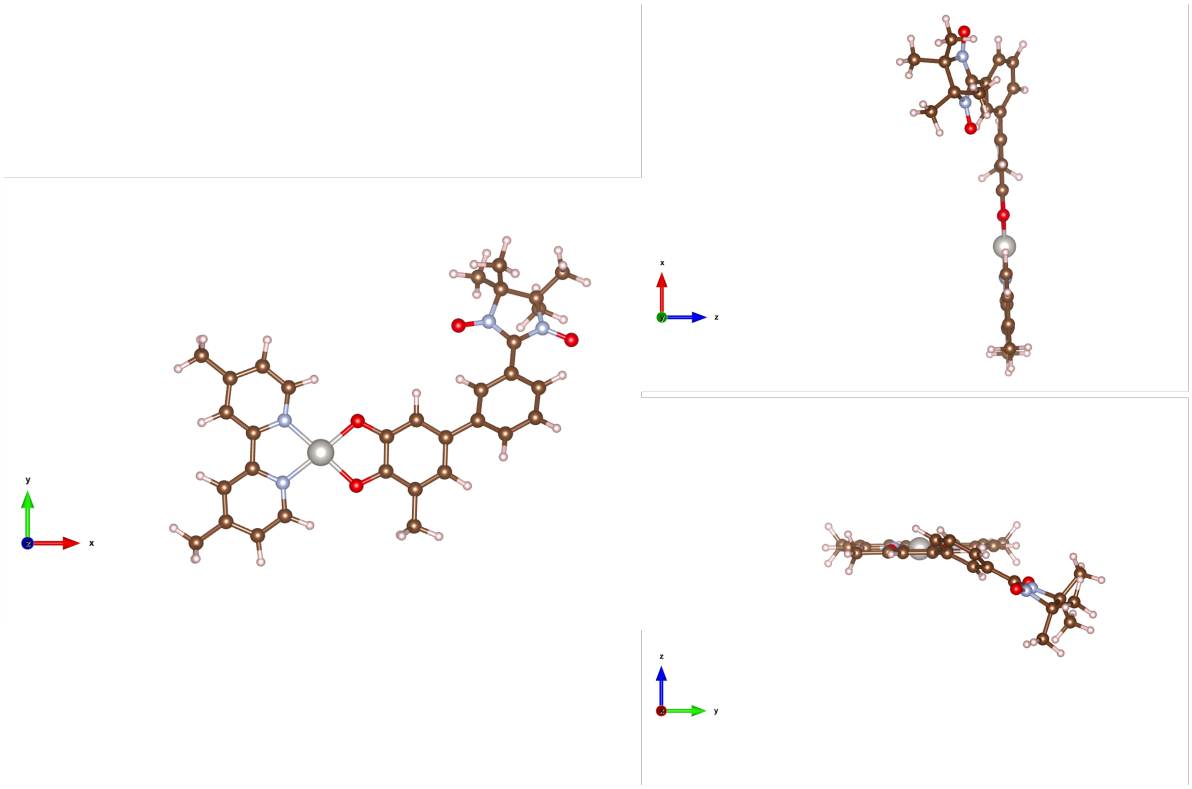

Figure S1: The optimized structure of bpy-Pt-CAT-*m*Ph-NN, viewing from three axes.

The optimized geometry of bpy-Pt-CAT-*m*Ph-NN:

C	-0.83374890900461	-1.14215981335407	6.41044945774216
C	-1.41002695040606	-2.43639816490032	6.36112003344654
C	-0.90966981990668	-3.41161657498401	5.47507952436797
C	0.17240503483522	-3.05694296736665	4.66617735487453
C	0.76394274070416	-1.77275579342790	4.70153458134913
C	0.24419148333855	-0.81169817436314	5.58405429646364
O	-1.36608394742845	-0.26801725179184	7.29158327030139
O	-2.44408445260367	-2.68401978331555	7.19091200499492
C	-1.54453542931088	-4.77496515475433	5.41715211698385
C	1.91252280394140	-1.45101943990935	3.82323432126599
C	2.08689563654435	-0.15359679396218	3.31183873749852
C	3.17319874681630	0.16800675827873	2.47298801088807
C	4.10675333276881	-0.83741656120578	2.13691071052946
C	3.94222595461112	-2.12160701463748	2.65154634395384
C	2.86559834859168	-2.43040473459600	3.48217909376448

C	3.32688330480554	1.52393164744992	1.94961865786128
N	2.75317099905086	2.65067915753488	2.46968635604612
C	3.28782820073090	3.90918245979930	1.80778528456703
C	3.85894160591529	3.33047971840031	0.47825845369817
N	4.07464053708406	1.87648385273914	0.86063296516481
O	4.75044376800321	1.10931497953643	0.09620588322776
O	2.00162743135814	2.74041369480768	3.49743784623817
C	2.85579202657496	3.31413729691686	-0.68741448931678
C	4.35530644249668	4.46486401240692	2.76557648354908
C	2.15309318152303	4.91878660689561	1.65256830018470
C	5.18384592958087	3.92942782798903	0.01201442133498
Pt	-2.87365273369804	-1.08416425623153	8.29885385295929
N	-3.33469313905037	0.48579878286884	9.42195702259568
C	-4.38002819019511	0.32129006306514	10.30542645668835
C	-4.77362202888575	1.37822329595860	11.14049265202213
C	-4.12433615252213	2.60816947917786	11.09749778189236
C	-3.05787859438777	2.74036838716024	10.17843442767528
C	-2.69484546680053	1.68037119231053	9.37042509874892
N	-4.38614306803482	-1.84157152751631	9.34144222700826
C	-4.85956537145532	-3.10539014558409	9.20839726847413
C	-5.91566974893491	-3.57699737709906	9.96393611158500
C	-6.54523586949368	-2.74086154129001	10.91463020193505
C	-6.05159101526218	-1.44625522059299	11.04247632907730
C	-4.97661478551937	-0.99877681062603	10.25962346742691
H	0.54922214349954	-3.79538645104718	3.95505546183894
H	0.68525132286634	0.18309560241579	5.66171536281898
H	-2.61079470824654	-4.70962833445799	5.14937247321550
H	-1.49741086979145	-5.28013905415666	6.39464811288209
H	-1.04064785576502	-5.40963464685436	4.67597849335154
H	1.36300639463678	0.61997999054967	3.55554593336788
H	4.93706190889222	-0.60398142526144	1.47596983995300
H	4.67383193001550	-2.89324457019983	2.40481863777781
H	2.77250902994425	-3.43605757258338	3.89524876930445
H	1.89055304484590	2.88084056238102	-0.39285910333608
H	3.27432525323976	2.70323390392367	-1.49817914359369
H	2.68319124173413	4.32973479860398	-1.06805281154524
H	5.18101881948775	3.75584014655672	2.91257653735771
H	3.88525860256827	4.65336417383933	3.73983365648589
H	4.76697305999072	5.40992814170690	2.38663282304694
H	1.32376463888035	4.52488168841100	1.05377387241095
H	2.52903757105101	5.83510055581019	1.17615572658812
H	1.76203057780848	5.17525594854646	2.64480621554732
H	5.95931486275584	3.87938898966683	0.78506223371700
H	5.04014598933392	4.97991936781950	-0.27732302289603
H	5.53997232520887	3.37059880230470	-0.86203466326208
H	-5.60319337350650	1.22710789098374	11.83241181908406
C	-4.52987777462223	3.75418794543282	11.98220048022882
H	-2.50807247450955	3.67851214200525	10.09491918679202
H	-1.87976214067375	1.73571354860776	8.64819842041329
H	-4.34487896817785	-3.71360889452020	8.46426541674286
H	-6.25446376151358	-4.60272910458392	9.81390496311008
C	-7.69479210055456	-3.24013531418048	11.74524604032779
H	-6.50468637667970	-0.76327964941932	11.76221853345432
H	-4.85339770377991	4.61976460865810	11.38354141309454
H	-3.68574517693492	4.09200949499440	12.60274663259169
H	-5.35455925127003	3.47588425487981	12.65085063128441
H	-7.39124937894406	-4.09805440699851	12.36510010719453
H	-8.52354247289173	-3.58373614794077	11.10737473157810
H	-8.07948616527301	-2.45818109768098	12.41240330000352

1.2 bpy-Pt-CAT-2Me-NN

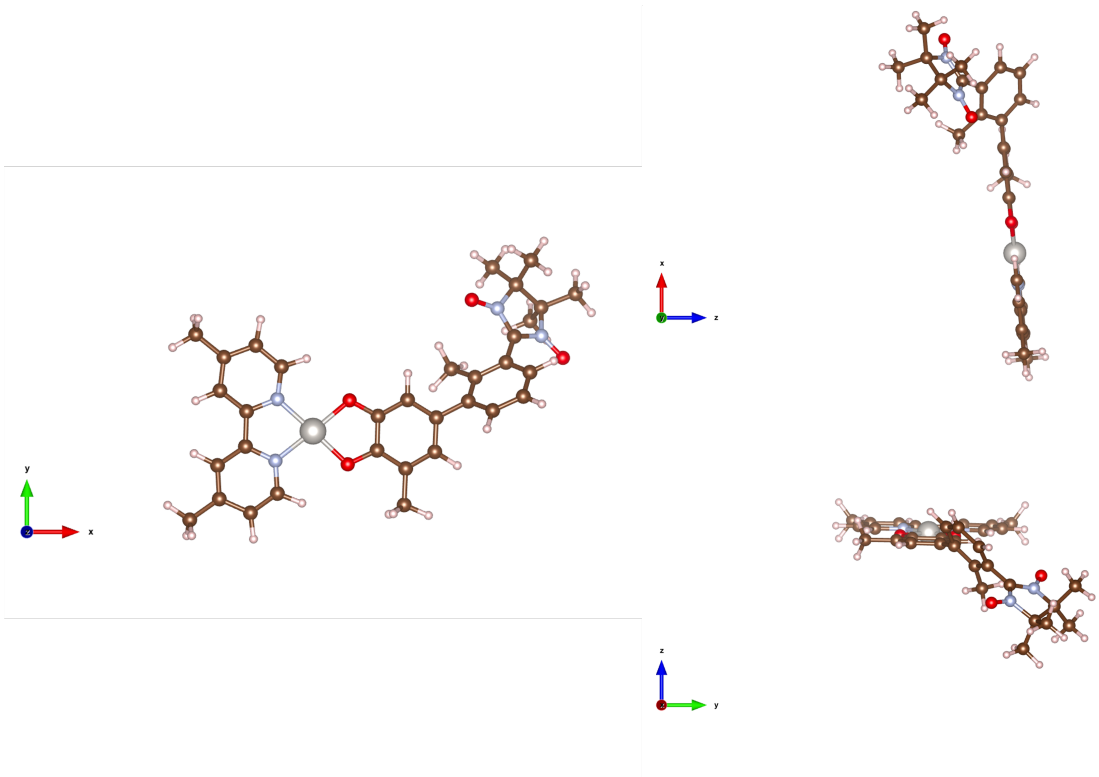

Figure S2: The optimized structure of bpy-Pt-CAT-2Me-NN, viewing from three axes.

The optimized geometry of bpy-Pt-CAT-2Me-NN:

C	-0.65660963532775	-1.19907164996233	6.57981655645157
C	-1.21741199634606	-2.48881414771701	6.40568821417162
C	-0.67725368720519	-3.38752037393325	5.46497307546896
C	0.42686124047087	-2.95974959207474	4.72146974935671
C	0.99777283801622	-1.67619367515134	4.87591984396139
C	0.44448817634521	-0.79462303356075	5.81687092300216
O	-1.22829665122651	-0.40143949466245	7.50820264728945
O	-2.27853719687007	-2.80933100749819	7.17585999448527
C	-1.28951547175610	-4.75068724673080	5.28578596698577
C	2.19938403856903	-1.30210799902009	4.08176119209835
C	2.27306948177258	-0.10737919317349	3.32031232532935
C	3.47823120630588	0.17755851730964	2.63296120282494
C	4.55335684909737	-0.72623788055428	2.64038485013374
C	4.45809884828057	-1.90965683584147	3.36508375151516
C	3.29636459678757	-2.18276015238128	4.08424871185112
C	3.65009245687021	1.42058905968436	1.87195454239996
N	3.48142293768094	2.67808168979241	2.35871777007551
C	3.97552619741512	3.72683947111963	1.37264898849183
C	4.02367682787397	2.90255892869964	0.04423903871949
N	4.08836113634249	1.48207584523208	0.58135132877177
O	4.35621343362858	0.49987735204230	-0.18560241504552
O	3.14922558172912	3.00565572538769	3.54554831071835
C	2.73678219608955	2.97450457821088	-0.79501735290934
C	5.35506330286986	4.16411158032579	1.89175160852566
C	3.01884267151129	4.91644397899243	1.37992886438944
C	5.23479498675585	3.15990252528704	-0.84959253927356

Pt	-2.76312379605036	-1.30773667892656	8.39144900795491
N	-3.28744545023961	0.16046638245380	9.62080502443252
C	-4.36621232301764	-0.08594371619838	10.44319084280674
C	-4.80853844472833	0.89546128461976	11.34320981571830
C	-4.17501921975466	2.13144523726623	11.42766617640082
C	-3.07238301514330	2.34845548772269	10.56953281942265
C	-2.66170364492537	1.36136486227699	9.69468372838726
N	-4.30466691900554	-2.16216042573209	9.30776080086149
C	-4.75458441046968	-3.41569221277142	9.05254737117056
C	-5.83421407063635	-3.95795849975330	9.72219100311656
C	-6.51374609981798	-3.20919747192690	10.71073588019469
C	-6.04327482515829	-1.92458184778507	10.96475434413427
C	-4.94334841396152	-1.40373594394834	10.26594134939097
H	0.85043417606611	-3.63688140460559	3.97585110181752
H	0.87373654158559	0.19384199077687	5.98608456777512
H	-2.34725503455437	-4.67901633309515	4.98739230593258
H	-1.26759414559344	-5.32505729064635	6.22519251394680
H	-0.75249624442855	-5.32337319714777	4.51795214892213
C	1.08242197231897	0.80274784892973	3.15935651854805
H	5.45391123402840	-0.49486634128814	2.07233531584831
H	5.29308454767061	-2.61172226040957	3.38093237150844
H	3.22769318075287	-3.09513814911273	4.67939257155575
H	1.83999667678108	2.79117908117113	-0.18830000151389
H	2.78858037419979	2.20357712114778	-1.57513570274941
H	2.63891572811286	3.95603300815628	-1.27794017680267
H	6.06651738987601	3.32784397820884	1.91387977173168
H	5.23778810498285	4.54324730652773	2.91537864947181
H	5.77164313116096	4.96426982867057	1.26559477496301
H	1.99983551350660	4.63513549619285	1.09042698642400
H	3.37974238969342	5.69396467405898	0.69213061556592
H	2.98064623925310	5.33611247132108	2.39306179027790
H	6.18377139800253	3.03287420735165	-0.31591817971481
H	5.19254555448918	4.18042707843302	-1.25535307607386
H	5.21922951212562	2.44995415575889	-1.68589628928927
H	-5.66341107564626	0.68045558011005	11.98549314800878
C	-4.63152621386000	3.19651567316747	12.38565231753155
H	-2.53228303051339	3.29572593929068	10.58660618404812
H	-1.81795508933334	1.48306202667025	9.01487615480215
H	-4.20118801896264	-3.95570516151221	8.28401642968206
H	-6.15230784555481	-4.97168590761961	9.47596056717405
C	-7.69113446759927	-3.78771157542978	11.44527651688519
H	-6.53303388977628	-1.30675460075118	11.71836432460542
H	-4.89577691299282	4.12190252603035	11.85118949891938
H	-3.83268131782194	3.45551441204974	13.09770970926653
H	-5.50837356546251	2.87317381647118	12.96118409935196
H	-7.41292080865710	-4.71535592998388	11.96862447469688
H	-8.50318145688315	-4.04535682757822	10.74781703400036
H	-8.09080472285921	-3.08461114559797	12.18731000930391
H	1.00666641970186	1.15280514279106	2.11853979601120
H	1.17580548709158	1.69941171939879	3.79045689123973
H	0.15131453632712	0.28729761497326	3.41976895254570

1.3 bpy-Pt-CAT-4Me-NN

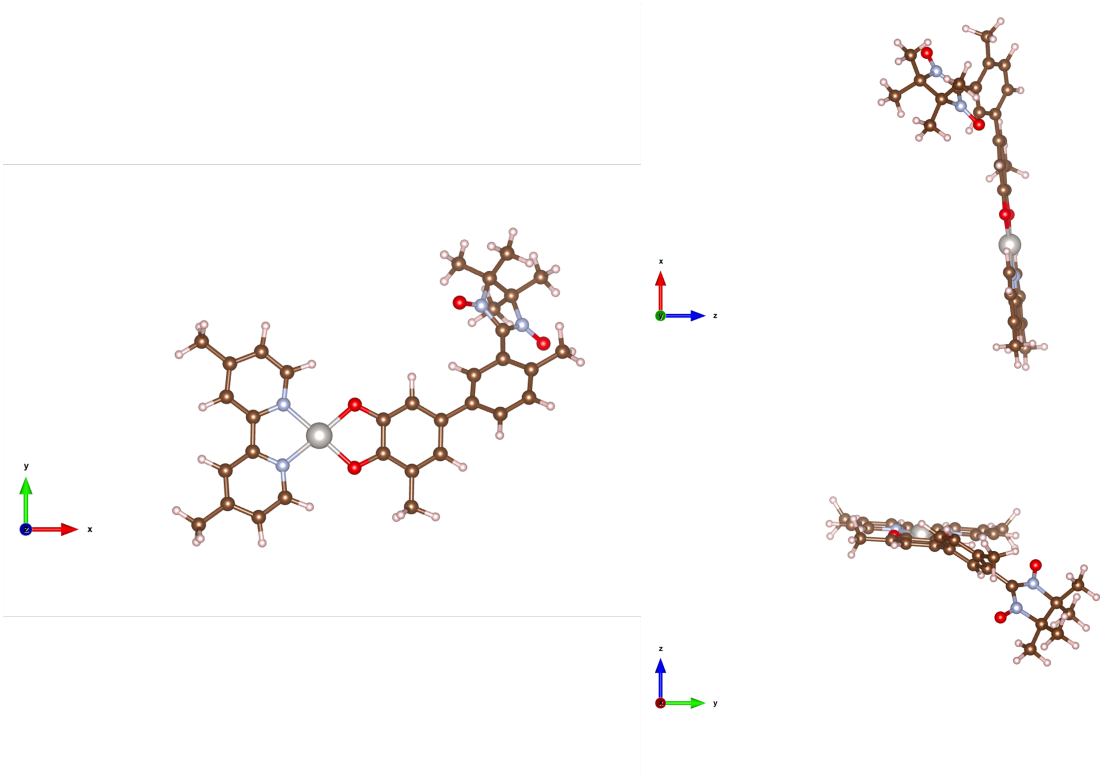

Figure S3: The optimized structure of bpy-Pt-CAT-4Me-NN, viewing from three axes.

The optimized geometry of bpy-Pt-CAT-4Me-NN:

C	-0.77288901739502	-1.15134508523469	6.40188952991323
C	-1.36297462247200	-2.43838007663102	6.33193353416553
C	-0.84578211166122	-3.41905334000169	5.46154146451104
C	0.26387632165808	-3.07591927754986	4.68525671078420
C	0.86689413775393	-1.79802913055466	4.73956562358862
C	0.33353721916865	-0.83261824548469	5.60910459188042
O	-1.32070790405756	-0.27249063097209	7.26857013283297
O	-2.42623842318462	-2.67399321645104	7.12797787343617
C	-1.49228675204594	-4.77600994430102	5.38504826841930
C	2.03944917243753	-1.48288796062833	3.89326464754913
C	2.22947154754645	-0.19692279064747	3.36397281820469
C	3.33298522461791	0.11889133277617	2.55660581080199
C	4.32241310150104	-0.85288655247787	2.27558195111770
C	4.12163262016290	-2.13562783863789	2.80394012604762
C	3.01306603233642	-2.45153070831940	3.58559263405604
C	3.41619490514960	1.48458537257510	2.02644312205524
N	3.29045956135730	2.61330510512779	2.78297248306195
C	3.57140292676077	3.86100506553500	1.96218877369892
C	3.37358811401878	3.31919702373184	0.50827512435586
N	3.55579796682977	1.82330196048437	0.71833046581467
O	3.62577389053101	1.03081079428932	-0.27936323968764
O	3.14204887118171	2.67713278077453	4.04709921446809
C	1.94667597774218	3.48836851683308	-0.03968665735204
C	5.01745172489104	4.26517294879293	2.29401120413209
C	2.61516560868909	4.97240910262813	2.38886887411352
C	4.38455825293305	3.81115901802389	-0.52479568665246

Pt	-2.86942732225209	-1.07117789700221	8.22646088550659
N	-3.34186166835769	0.50136495221726	9.34099965326454
C	-4.41879921485539	0.35073888193466	10.18837189217246
C	-4.82197204241631	1.41055910635668	11.01534283972272
C	-4.15013170011280	2.62897632609868	11.00110152440198
C	-3.05096930725838	2.74677109160509	10.11924985393319
C	-2.67966829780548	1.68461012149940	9.31798016276471
N	-4.42649285626540	-1.80865360088378	9.21654105605141
C	-4.91531536175463	-3.06424231477371	9.06281824193589
C	-6.00469454310008	-3.52073518368322	9.77935138138642
C	-6.65365817870634	-2.67708827658469	10.71026948825514
C	-6.14375178888436	-1.39120310653246	10.85996996275172
C	-5.03491185421958	-0.95902686306976	10.11667770728540
H	0.65491473794478	-3.81729489793483	3.98481098217279
H	0.78932183197225	0.15393009723933	5.70686303595367
H	-2.55141868789094	-4.69972540620320	5.09312611436714
H	-1.47233658256505	-5.28400655263276	6.36204334165397
H	-0.97745819075102	-5.41364167305633	4.65403533777373
H	1.48712396309245	0.57538813393214	3.56472504043723
C	5.56567862091411	-0.53922195307083	1.48818045230006
H	4.87506901594219	-2.90285027431504	2.61034908762246
H	2.91808367039955	-3.45710461092095	3.99884725541223
H	1.18958166406906	3.13155360405425	0.67131216166552
H	1.85715860803328	2.89931149991921	-0.96168645947296
H	1.74113538664698	4.54148113329934	-0.27359450159866
H	5.73573815256216	3.48329207789881	2.01349743051669
H	5.09391775463157	4.43024489304319	3.37691275995287
H	5.29127281456946	5.19502783967981	1.77777484865160
H	1.56357449449213	4.69297863131021	2.25679860989200
H	2.81435712484312	5.88350166994071	1.80735065246196
H	2.77589777288889	5.19364137485904	3.45138575292303
H	5.42080405236521	3.63105005422838	-0.21613679913524
H	4.25049506541523	4.88794046820665	-0.69926187906393
H	4.21456478783062	3.28035068649057	-1.46985055366462
H	-5.67673056307011	1.27067715439823	11.67838098144488
C	-4.56293389829351	3.77682140520159	11.88006409133195
H	-2.48194700360134	3.67524300237846	10.05981352662868
H	-1.83950720098347	1.72907941716624	8.62431171458452
H	-4.38487054366056	-3.67853134082199	8.33492132547726
H	-6.35464506405674	-4.54037062940547	9.61416085753829
C	-7.83992765066538	-3.15982966147435	11.49787974253912
H	-6.61022518144992	-0.70284383138117	11.56588834485324
H	-4.82067590939307	4.66216732688759	11.27864908246022
H	-3.74275667753150	4.07423339692017	12.55161358293003
H	-5.43253537265948	3.51981590246256	12.49843379234336
H	-7.57353454404183	-4.02672994530287	12.12226393178079
H	-8.65244529938058	-3.48435830510467	10.82979684393266
H	-8.23316023428172	-2.37481179729379	12.15643113777950
H	5.31861743158446	-0.29489518438231	0.44359992866881
H	6.25675148208297	-1.39241427864558	1.49966391602064
H	6.09693996153352	0.32936311156723	1.90885048411437

1.4 bpy-Pt-CAT-6Me-NN

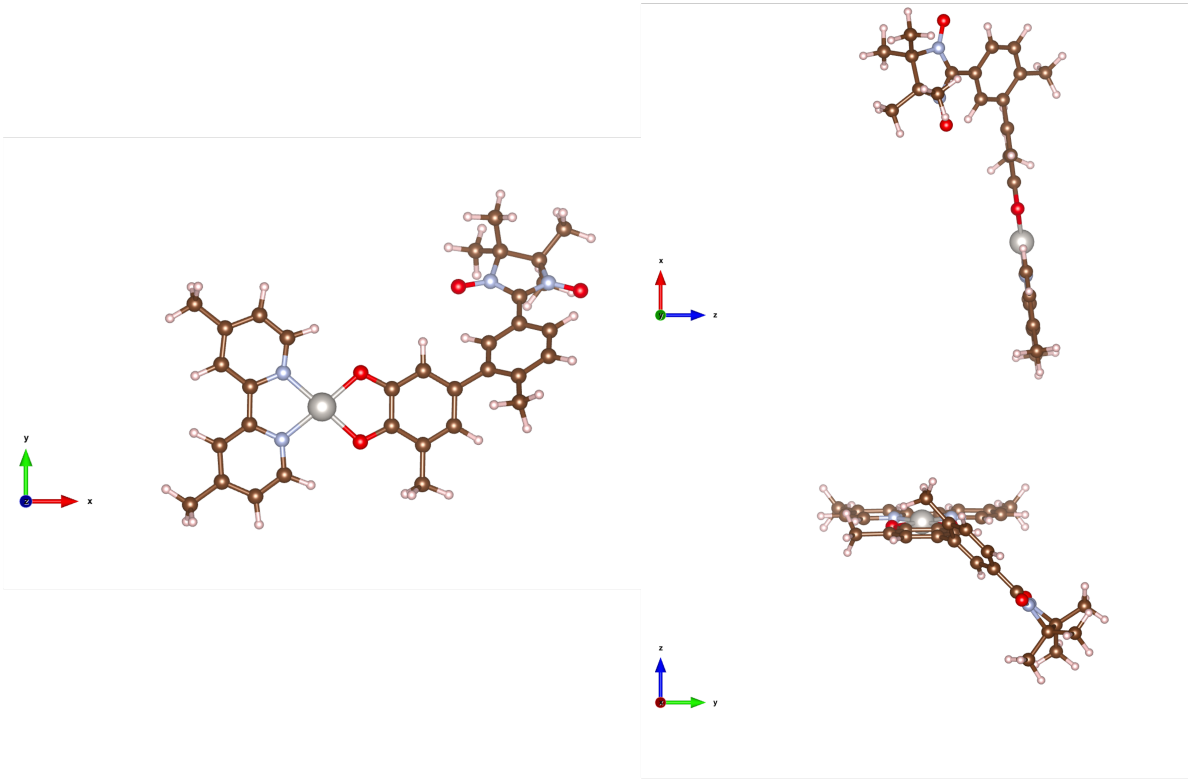

Figure S4: The optimized structure of bpy-Pt-CAT-6Me-NN, viewing from three axes.

The optimized geometry of bpy-Pt-CAT-6Me-NN:

C	-0.65904718705778	-0.88364238977494	6.41351493452284
C	-1.38687552394365	-2.07563099933518	6.17499185266116
C	-0.96577908162829	-2.98661574659025	5.18560602832310
C	0.19371603385422	-2.67571812423109	4.46829612786089
C	0.93404266741663	-1.49377213274123	4.69313836915224
C	0.49116276850023	-0.59203049789696	5.67269302296299
O	-1.12552812529728	-0.06262961675774	7.37838430702305
O	-2.48679748336960	-2.28865446903337	6.92848686846018
C	-1.75968347719683	-4.23839728556601	4.92449354773135
C	2.13677307808412	-1.16761861444623	3.87902134260334
C	2.20265085598536	0.09826958941774	3.27458863559654
C	3.29475357947266	0.49192364767569	2.47613045181449
C	4.35494169926927	-0.42176582300611	2.29362351637227
C	4.30249376671215	-1.66314659874449	2.91639121575817
C	3.21841055210563	-2.06866796277867	3.71044602083431
C	3.32180838970958	1.80731625782904	1.84439348830393
N	2.55958525878679	2.88363198260798	2.20534660319204
C	2.97562388011300	4.14091921482200	1.46200164500324
C	3.72984520801252	3.53198317405867	0.24245907172474
N	4.11275293248627	2.16782418463810	0.78837565747438
O	4.95380318137207	1.44081781481817	0.15949538960221
O	1.71623054429392	2.95681148455524	3.16101345472560
C	2.83821838673323	3.25850561999935	-0.98070593017364
C	3.87402104083568	4.92577444078929	2.43256279040131
C	1.73331659404687	4.96298659324955	1.12735380041850
C	4.98968475239257	4.27629727049891	-0.19268942256725

Pt	-2.77504345145555	-0.79111853935576	8.21317193417389
N	-3.09226828423126	0.68397646118114	9.50173430312327
C	-4.19465839072544	0.55860139759025	10.31933565159521
C	-4.49397145603901	1.55576508911703	11.26078695908757
C	-3.69259801255529	2.68600742037238	11.38938428602054
C	-2.57158793484659	2.78058797471555	10.53278424807862
C	-2.30422170943381	1.78151385043304	9.61725111390507
N	-4.42548113999844	-1.45764744049786	9.09748937770818
C	-5.05017218922514	-2.62253714011926	8.79387548305961
C	-6.19578248859475	-3.03376775884910	9.44737319821883
C	-6.76100042503685	-2.23824659306600	10.47080832754468
C	-6.11238920724020	-1.04518459145468	10.77389168867437
C	-4.95050670684194	-0.65661849233694	10.09036668731065
H	0.51411221517733	-3.36130164921203	3.68108932960339
H	1.03790687413053	0.33018433699047	5.87594646502024
H	-2.79656070941508	-4.00284667909720	4.63776679847737
H	-1.81983360524767	-4.87064759154154	5.82440320065312
H	-1.30379149927697	-4.82836337024756	4.11817646931447
H	1.37692908696926	0.79088687449107	3.41971148738790
H	5.20240180983396	-0.14957143165937	1.66995805516047
H	5.14545928237100	-2.34771736051704	2.79245153457614
C	3.27016562762653	-3.42054938338573	4.37815128283740
H	1.92546591924113	2.71144951855953	-0.70875434993856
H	3.40608522541468	2.64740661067030	-1.69469008882868
H	2.55177455618715	4.19704727394697	-1.47394739312819
H	4.77216915881081	4.35801491547431	2.71084773518713
H	3.30095114264540	5.13301812134258	3.34605771568786
H	4.18474765805819	5.88180964811314	1.99038799856322
H	1.02350457181206	4.41149085799992	0.50027062591444
H	2.02322096843373	5.88601217655586	0.60572463430933
H	1.22206035959685	5.23363358534394	2.05941171789351
H	5.69916394661371	4.41594619426097	0.63111638864559
H	4.72046613914202	5.26202125306745	-0.59769238693438
H	5.49371128568716	3.70110931692669	-0.97916673092660
H	-5.37080349188947	1.43789585490335	11.89880710238620
C	-3.99449989699859	3.76749787806925	12.38931314547528
H	-1.90403168743241	3.64156815433577	10.58274585146774
H	-1.45255356564003	1.81103466939442	8.93693000802063
H	-4.57979096557694	-3.20307866483915	8.00000079201400
H	-6.65538841769522	-3.98033554912531	9.16070722208299
C	-8.00696085086329	-2.67283234628571	11.19139129406381
H	-6.50931943032584	-0.39627937833159	11.55567398858695
H	-4.16833153317070	4.73170324146453	11.88698369179563
H	-3.14938180693554	3.91427068446392	13.07925111662983
H	-4.88433642776987	3.52961641598208	12.98619552572047
H	-7.85677563964776	-3.64220241209960	11.69128201579050
H	-8.84504897901888	-2.80162980984014	10.48919990406621
H	-8.30891924388950	-1.94096232447852	11.95146369884367
H	4.31307134829358	-3.72596327633070	4.54370513293308
H	2.79936116736001	-4.20045159862109	3.75828603961750
H	2.74293651192365	-3.41898740853148	5.34114693274739

1.5 bpy-Pt-CAT-2,4,6Me-NN

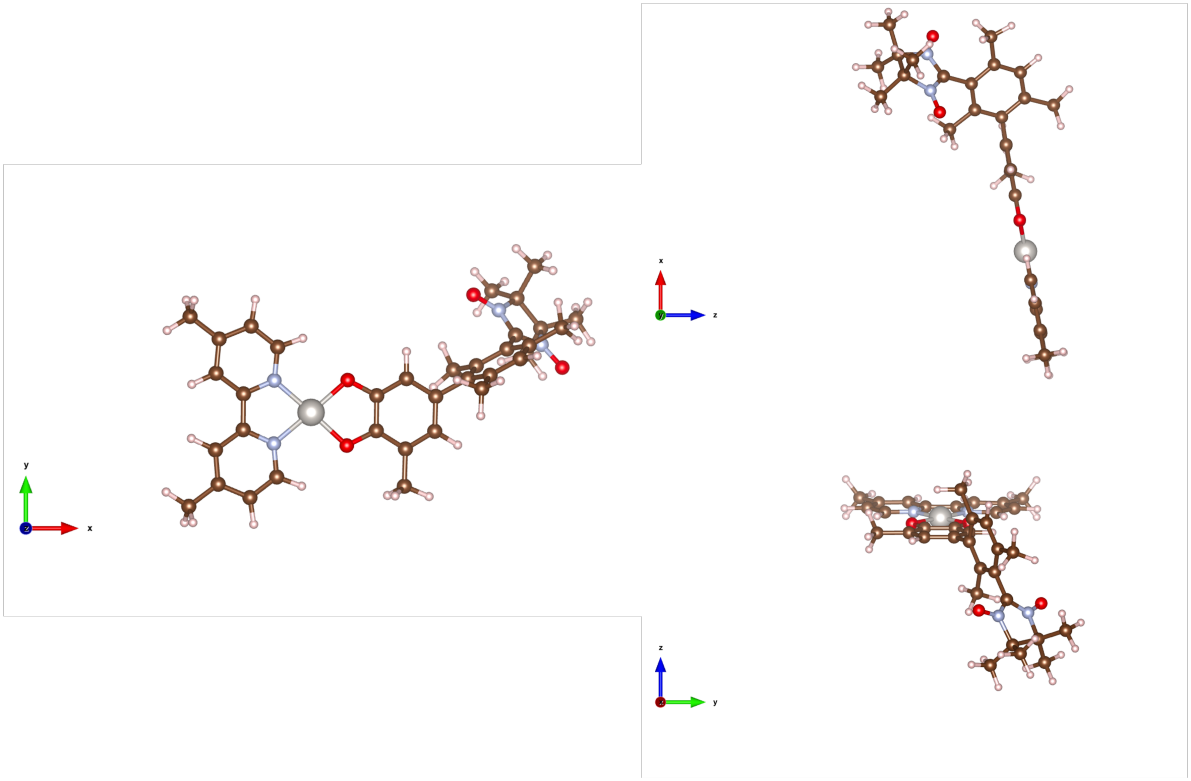

Figure S5: The optimized structure of bpy-Pt-CAT-2,4,6Me-NN, viewing from three axes.

The optimized geometry of bpy-Pt-CAT-2,4,6Me-NN:

C	-0.55747617124411	-0.85515289772831	6.56871255597946
C	-1.34279228181384	-1.92839035023393	6.08064039900956
C	-0.94594648106758	-2.65462821307411	4.94141742539447
C	0.25141158320759	-2.28134778798462	4.32019297356622
C	1.04738789493733	-1.21666601883768	4.79196274696432
C	0.63535623694609	-0.50024099570036	5.92336430185936
O	-1.01263395861007	-0.20984597546726	7.66452620988880
O	-2.47842736271875	-2.21746555215416	6.75285737058914
C	-1.79907396115271	-3.78515071003836	4.43246925072090
C	2.32895025537218	-0.87061222586991	4.09864448059709
C	2.38840946193111	0.20125935634868	3.18249802020722
C	3.61621714038816	0.50347268093773	2.54587609458812
C	4.77768705322681	-0.25442604166046	2.80144714848721
C	4.68152289324811	-1.30966963128579	3.71106301989663
C	3.48875517567289	-1.63269152091199	4.36531379951970
C	3.68649250337912	1.63254748344120	1.60509283833135
N	3.49428377533224	2.93812937991235	1.93572566925555
C	3.82763196268094	3.86220617108018	0.77470990419951
C	3.78585610017672	2.86558224907901	-0.43171793166513
N	3.96555341047592	1.53228445915453	0.27780477696329
O	4.19153650591330	0.46237579010288	-0.37900248948282
O	3.23214794468763	3.40404774916386	3.09316254900906
C	2.42179728416645	2.78200423977418	-1.13612893124352
C	5.22555865225547	4.42630228135367	1.07797186476093
C	2.81394591293712	5.00325786481961	0.72794644267736
C	4.89152283940159	3.03841539465530	-1.47065378472830

Pt	-2.72652158765139	-0.99574863386120	8.30359075237283
N	-3.03183746572795	0.19434787435148	9.86430246746757
C	-4.17085454333209	-0.04793151315453	10.60336458953735
C	-4.47012235984012	0.74386902687720	11.72203201327177
C	-3.63337813561968	1.78507504421377	12.11150089747362
C	-2.47510483281647	2.00460028348490	11.33071462223504
C	-2.20874175713888	1.20676478012472	10.23472926343822
N	-4.43297084905507	-1.75109497794639	8.98194080295174
C	-5.08537016587188	-2.79896242217497	8.42042184290997
C	-6.26828307389370	-3.28879078489839	8.93877633975057
C	-6.84269164062077	-2.70173976996178	10.08967828043066
C	-6.16502090826469	-1.62685187884724	10.65662397490443
C	-4.96467671948505	-1.15320761984308	10.10456700363516
H	0.57564933816441	-2.82880364020248	3.43157005761195
H	1.22832200400805	0.33066914589399	6.30955349920356
H	-2.80930683490915	-3.43605093160335	4.16664884786020
H	-1.92984993433712	-4.56524485222471	5.19893916057825
H	-1.34877410247690	-4.24701174306628	3.54363849999268
C	1.15657071798614	1.00773172950704	2.85387041774284
C	6.09505838121392	0.05709911968308	2.13978392930542
H	5.57796990936556	-1.89752189071793	3.92630943872992
C	3.46253599872134	-2.77918260206033	5.34564270456666
H	1.60029463763131	2.63736135772653	-0.42187346759614
H	2.43645771609890	1.92439848489914	-1.82167966332687
H	2.22552255273906	3.69224004784747	-1.71843952766336
H	5.98406692479733	3.63410183630091	1.13009842324949
H	5.19286017294593	4.93643013927664	2.04973667293657
H	5.52844248988251	5.15145644332818	0.31076155983648
H	1.78703872177912	4.64839933596010	0.58387132579259
H	3.06603757413279	5.69557859658510	-0.08752691929933
H	2.85304696323146	5.55137091652728	1.67763362769268
H	5.89257597092718	3.01886304290111	-1.02474190877089
H	4.76096932698611	3.99038494588506	-2.00414516603141
H	4.82899857919074	2.21877298931072	-2.19739167999215
H	-5.37597369384102	0.53638684457257	12.29303911717223
C	-3.93706013866097	2.64488647898734	13.30703317461922
H	-1.77811877168564	2.80495983207589	11.58166046746743
H	-1.32939256787011	1.33838727902711	9.60365558227555
H	-4.60552217447753	-3.21987662919537	7.53656035757183
H	-6.74939339927372	-4.13443187562876	8.44590419119401
C	-8.12916216723342	-3.22519887548165	10.66566392260797
H	-6.56945306389614	-1.14142341409309	11.54563108904788
H	-4.02370333769603	3.70418180849233	13.02013570627139
H	-3.13134967972540	2.58100892237210	14.05460736532938
H	-4.87538147375454	2.34477384286609	13.79075398624148
H	-8.03332563293575	-4.28511325565033	10.94741260322506
H	-8.94575385264812	-3.16247942090643	9.92990703476097
H	-8.43093230024002	-2.66167984142733	11.55788213081241
H	4.47479836760703	-3.17017687694387	5.51559370669475
H	2.83307304160678	-3.60537521383465	4.98175488843665
H	3.03794155355491	-2.47067162573501	6.31208431711074
H	1.03255329001671	1.10503653764004	1.76410272543664
H	1.23799781897328	2.02490983271902	3.26807992671192
H	0.25424840737792	0.53865659793913	3.26018905349944
H	6.02782966558066	-0.08727716672052	1.05034523690694
H	6.88808233020991	-0.59460258823135	2.52941335554280
H	6.40032034052054	1.10005974815865	2.31962067291808

1.6 bpy-Pd-CAT-*m*Ph-NN

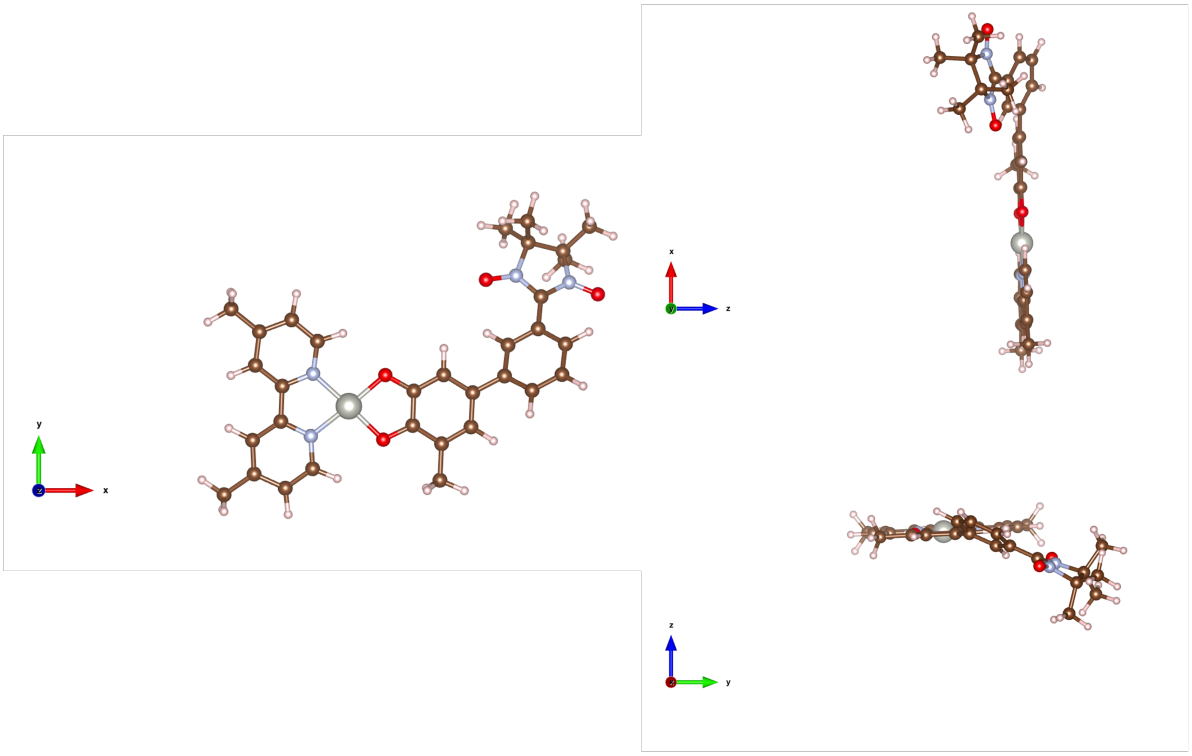

Figure S6: The optimized structure of bpy-Pd-CAT-*m*Ph-NN, viewing from three axes.

The optimized geometry of bpy-Pd-CAT-*m*Ph-NN:

C	-1.32302863915181	-1.05290301598668	5.19623095076296
C	-2.17707823899418	-1.97464289549025	4.53369139718054
C	-1.65851695131771	-2.86707767680223	3.57131529681378
C	-0.28854359151568	-2.81479173370605	3.30587265920850
C	0.57995468863992	-1.90604384805695	3.95435959601460
C	0.04490384910864	-1.02002696884031	4.90444630535673
O	-1.88496133500872	-0.23536095824062	6.11014454244106
O	-3.48342079470335	-1.95962181425492	4.85862643858633
C	-2.57883109348303	-3.82458509261248	2.86337772320683
C	2.02564245578899	-1.88852691827757	3.63428311624477
C	2.76365998113362	-0.69411252301129	3.70448284201573
C	4.13993360379560	-0.65781442136982	3.40272970437840
C	4.79319595053808	-1.84844889389286	3.01397081936293
C	4.06683942382300	-3.03582868536066	2.95301690198955
C	2.70659023394552	-3.06338080620817	3.25860210254195
C	4.88196409406402	0.59822894711147	3.48828956957162
N	4.50117742406185	1.70407535443213	4.19687173466959
C	5.60751118868851	2.74310884279567	4.24953141329171
C	6.47435283081693	2.31879654353865	3.02597117396882
N	6.07991169012619	0.85880899851067	2.88280691026153
O	6.75630000284565	0.08595904600267	2.12451294643324
O	3.45256860959649	1.85176970764474	4.90961211304065
C	6.07353988120873	2.99509002747694	1.70393033925403
C	6.29843635324316	2.55049180623026	5.61009349850778
C	4.99525265068636	4.13939409084790	4.17127729798533
C	7.98493494710988	2.41655659079538	3.22166918335300
Pd	-3.82548786303161	-0.58237262682030	6.23973870906992

N	-4.23320678329834	0.78664208345080	7.62902236860005
C	-5.54778409129484	0.86780546262919	8.01998772522532
C	-5.93735992623205	1.80028611608936	8.99424943451947
C	-5.00684335251196	2.65570090098264	9.57886941318894
C	-3.66536771044248	2.54205952755333	9.15025924997389
C	-3.31999163205826	1.60963204736888	8.18738921112745
N	-5.78895187659727	-0.87528801564946	6.42815329647401
C	-6.50193316729206	-1.78755228126145	5.73362517225448
C	-7.86559059689789	-1.94427818868390	5.91093607340998
C	-8.55678793675225	-1.13714687506575	6.84199063570734
C	-7.80912984200612	-0.20029178346234	7.55095161019652
C	-6.42687494831313	-0.07153370292127	7.34183803291003
H	0.11444093927530	-3.48033282461710	2.53930349486026
H	0.68261246414340	-0.32059683158662	5.44703663157640
H	-3.37136806957590	-3.28966737789267	2.31663143617149
H	-3.08742498216536	-4.49215322106623	3.57671775949308
H	-2.02370008336003	-4.44451409957291	2.14650186727549
H	2.26356562174672	0.22896796216057	3.98600587959713
H	5.84949022195898	-1.82667400283450	2.76004655772855
H	4.57584792913993	-3.95897794204755	2.66962531001306
H	2.16604484763580	-4.01078076103471	3.23115026632069
H	4.99080198845265	2.94154170030423	1.52817479889844
H	6.58273813656969	2.47845323410331	0.87962463914478
H	6.37897803110532	4.04998127720452	1.69754995426248
H	6.74504428443525	1.55150271608164	5.70349496320386
H	5.54658712939690	2.66745507927358	6.40184593996476
H	7.08462629046740	3.30256769390112	5.76054228602043
H	4.40357032786804	4.28505228919799	3.26017381879201
H	5.78934119589811	4.89862171980338	4.20218362876738
H	4.33314921171150	4.29009500373264	5.03271280960058
H	8.32730099325580	1.86832911252472	4.10684719172802
H	8.28265790885894	3.46990387540086	3.32051941846886
H	8.48819750403937	1.99145955040686	2.34457091167144
H	-6.98429313832947	1.85336848975787	9.29549529203011
C	-5.40187740658010	3.66322117544479	10.62276382910973
H	-2.88966856538888	3.18345045524463	9.57001551214251
H	-2.29954567762428	1.48168564983804	7.82235077858815
H	-5.92314186328855	-2.38601833946039	5.02839322790500
H	-8.39427838940317	-2.69633659162392	5.32417258850024
C	-10.03771329025800	-1.29258100395462	7.05068725192113
H	-8.30186614100445	0.44399376927844	8.28012432139892
H	-6.47434413482055	3.61091732576805	10.84978575576174
H	-5.17254482508567	4.68676363929924	10.28847147981247
H	-4.84524468136363	3.50021249896330	11.55828790812765
H	-10.28358703666313	-2.31285153822165	7.38311632156435
H	-10.58803815296417	-1.12045866150136	6.11299074961638
H	-10.41616807640204	-0.58848738976096	7.80270791086204

2 XMS-CASPT2 calculations for the structures without alkyl groups

In order to investigate the electronic and structural effects of the alkyl groups on the excited states, we also performed calculations for model structures without alkyl groups in the bpy and NN moieties, which we named bpy-M-NoMe. The energies are listed in Table S1, and the comparison of each excitation energy is shown in Fig. S7.

Table S1: Excitation energies of several low-lying states of bpy-M-NoMe model molecules calculated using XMS-CASPT2

	$^2T_1$/ cm^{-1}	$^4T_1$/ cm^{-1}	$^2S_1$/ cm^{-1}	^2LE/ cm^{-1}
bpy-Pt-NoMe	16149	16264	16849	17986
Pt-2Me-NoMe	15959	16050	16688	19009
Pt-4Me-NoMe	16006	16123	16697	18975
Pt-6Me-NoMe	16146	16237	16864	17499
Pt-2,4,6Me-NoMe	16408	16515	17144	18780
bpy-Pd-NoMe	14808	14941	15931	17244

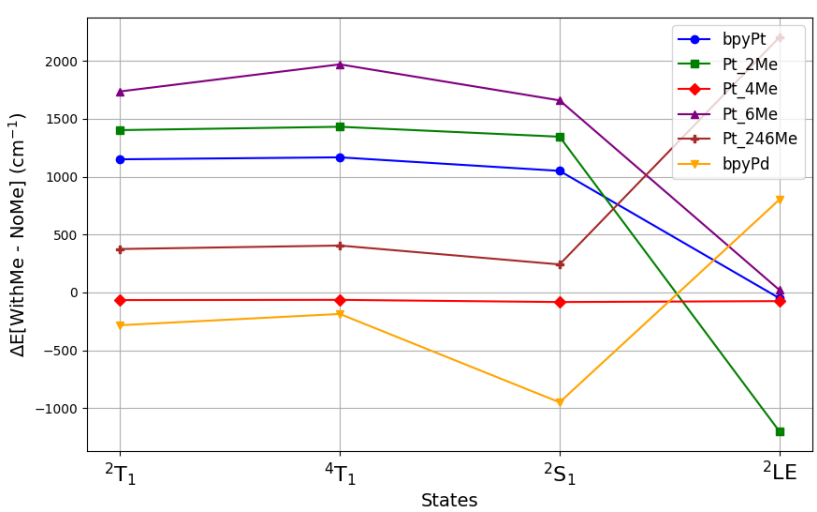

Figure S7: Energy differences between the structures with or without alkyl substituents

The results showed that the energies of the charge-transfer (CT) states increased overall with the addition of Me groups, whereas the energy of the doublet local excited (LE) state did not exhibit any systematic effect. Since alkyl groups are electron-donating, it is reasonable that they destabilize the acceptor's LUMO, thereby increasing the energies of the CT states.

3 Dependence of state energies on different CASPT2 IPEA shift values for bpy-Pt-CAT-*m*Ph-NN

We examined the energy variations of excited states under different computational settings for the CASPT2 method. Specifically, we investigated the effects of changes in the IPEA shift in CASPT2. In this section, all calculations were conducted on a model Pt molecule (bpy-Pt-NoMe), where the Me groups were replaced with H in the same manner as in Section 2 of the main text.

Table S2: Comparison of several low-lying excited states of bpy-Pt-CAT-NoMe under different values of XMS-CASPT2 IPEA shift. All conditions except for the IPEA shift are the same as those in Section 2.

IPEA / a.u.	$^2T_1$/ cm^{-1}	$^4T_1$/ cm^{-1}	$^2S_1$/ cm^{-1}	^2LE/ cm^{-1}
0	12491	12580	13320	14559
0.10	14083	14143	14818	16247
0.20	15492	15589	16199	17445
0.25*	16149	16264	16849	17986
0.30	16780	16911	17473	18500
0.40	17970	18130	18657	19469

* Same as the result in Section 3.1 of the main text.

4 Dependence of state energies on the number of states in CASSCF state-averaging

We also calculated the energy dependence of the low-lying excited states on the number of states included in the CASSCF state-averaging. Note that the energies listed in the table are those obtained using the XMS-CASPT2 theory. The structure used was bpy-Pt-NoMe, and all other computational conditions were identical, as in Section 2 of the main text.

Table S3: Comparison of several low-lying excited states of bpy-Pt-CAT-NoMe under different number of states in CASSCF state-averaging.

State averaging	$^2T_1$/ cm^{-1}	$^4T_1$/ cm^{-1}	$^2S_1$/ cm^{-1}	^2LE/ cm^{-1}
D3	14655	-	15525	-
D3Q1	15925	16071	16702	-
D4Q2	14227	14305	15072	16872
D6Q2	15408	15513	16117	17220
D8Q3*	16149	16264	16849	17986

* Same as the result in Section 3.2 of the main text.

The results of varying the number of states in the state-averaging are summarized in Table S3. Note that in the table, D denotes a doublet and Q a quartet. The D3Q1 state-averaging provides results that agree well with the experimental values for the CT states, but it is unable to include the LE state. Furthermore, in D4Q2 state-averaging, which is the minimal state averaging scheme that can include both the doublet and quartet LE states, the energies of the CT states were found to be underestimated by approximately 2000 cm^{-1}. After further testing, we found that the D8Q3 state-averaging yields good agreement with the vertical excitation energy. Consequently, we adopted this scheme for the subsequent calculations. It should also be mentioned that none of these calculations yielded the ^{4}LE state.

5 Active spaces of bpy-M-CAT-Linker-NN for electronic calculations

For the CASSCF/CASPT2 calculations, active spaces with thirteen electrons and thirteen π orbitals were selected, as mentioned in the main text. In this section, the converged natural orbitals are illustrated. Molecular orbitals were shown using the Avogadro software.[S2]

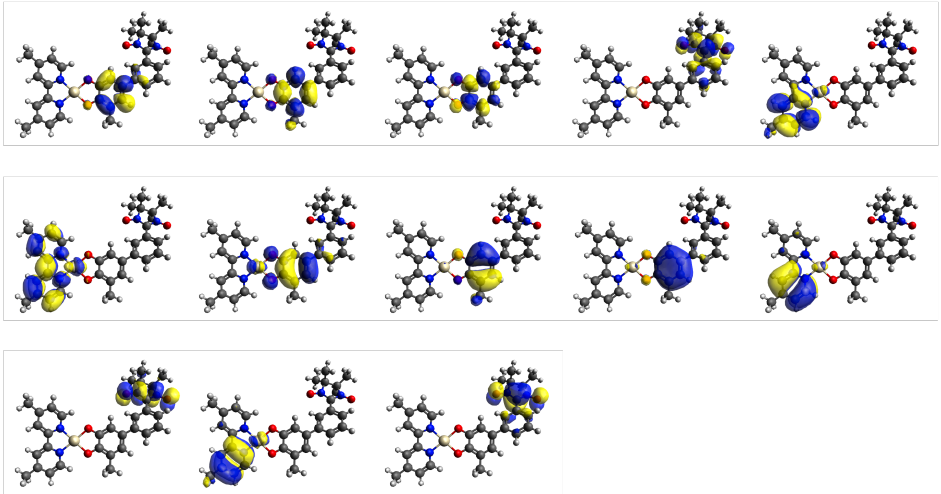

Figure S8: Illustration of CASSCF converged natural orbitals of bpy-Pt-CAT-*m*Ph-NN. The isosurface value was set to 0.02.

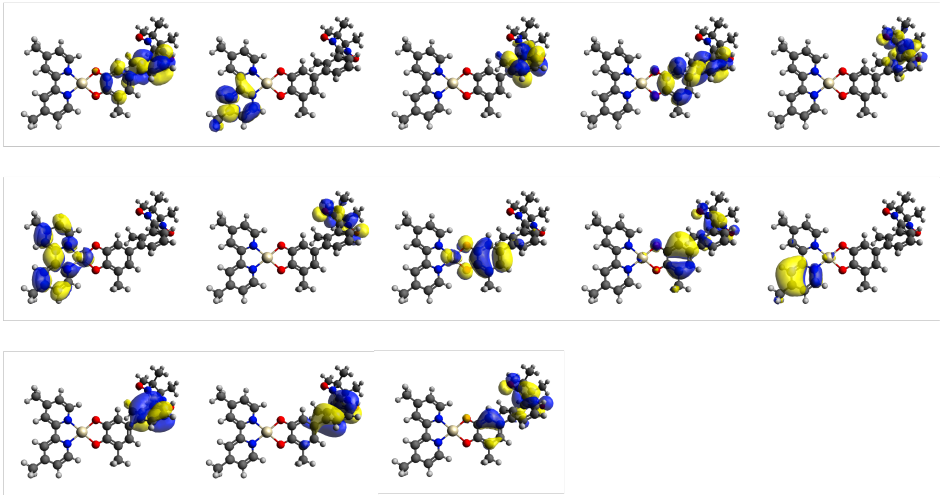

Figure S9: Illustration of CASSCF converged natural orbitals of bpy-Pt-CAT-2Me-NN. The isosurface value was set to 0.02.

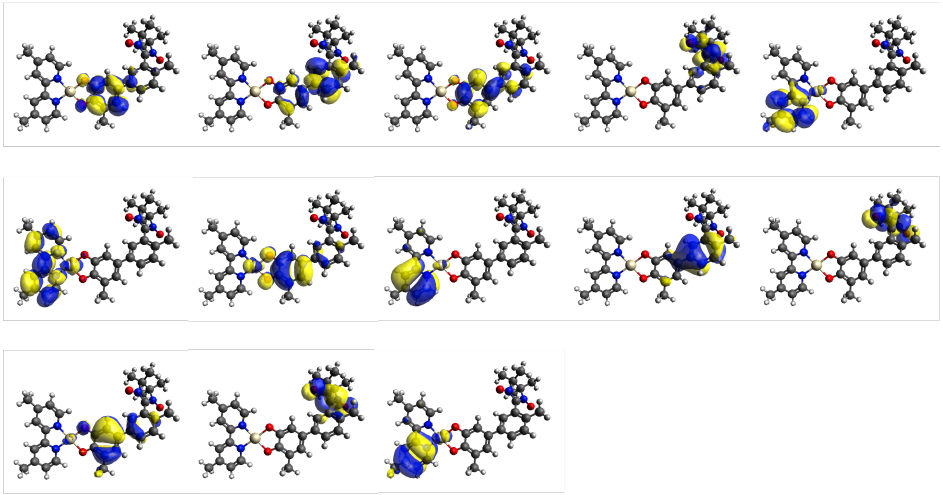

Figure S10: Illustration of CASSCF converged natural orbitals of bpy-Pt-CAT-4Me-NN. The iso-surface value was set to 0.02.

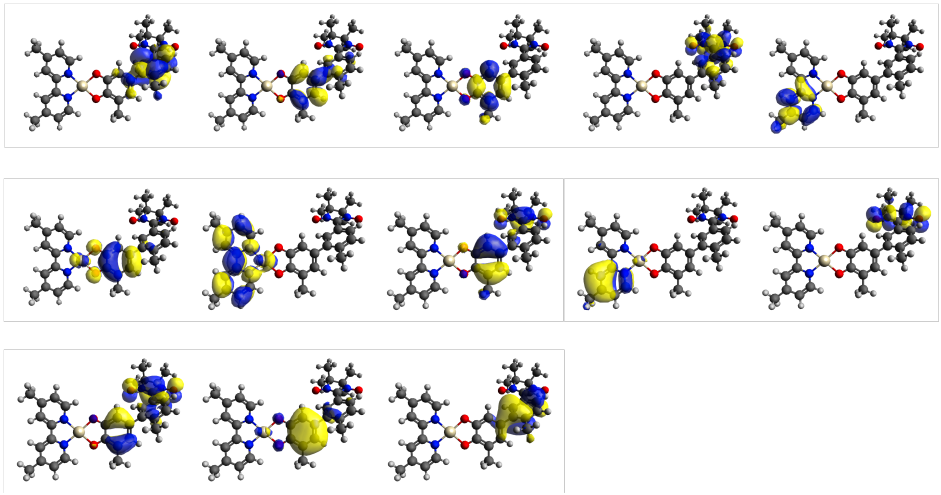

Figure S11: Illustration of CASSCF converged natural orbitals of bpy-Pt-CAT-6Me-NN. The iso-surface value was set to 0.02.

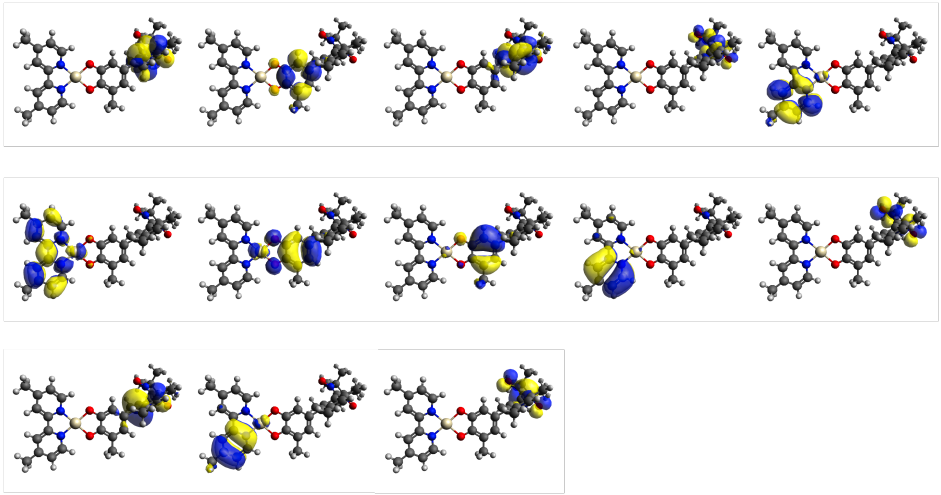

Figure S12: Illustration of CASSCF converged natural orbitals of bpy-Pt-CAT-2,4,6Me-NN. The isosurface value was set to 0.02.

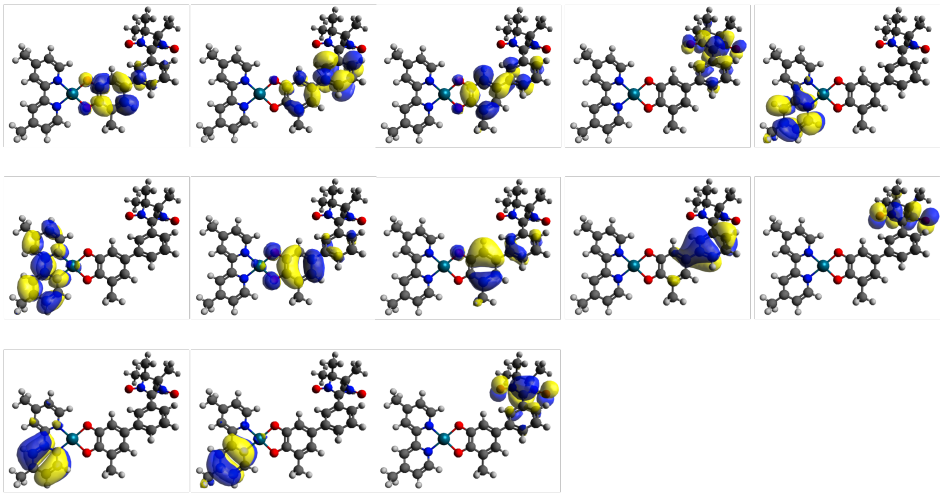

Figure S13: Illustration of CASSCF converged natural orbitals of bpy-Pd-CAT-*m*Ph-NN. The isosurface value was set to 0.02.

6 Spin density for each low-lying state

In this section, to facilitate a clearer understanding of the spin characteristics of each electronic state, we visualize the spin densities of each state obtained from XMS-CASPT2 calculations.

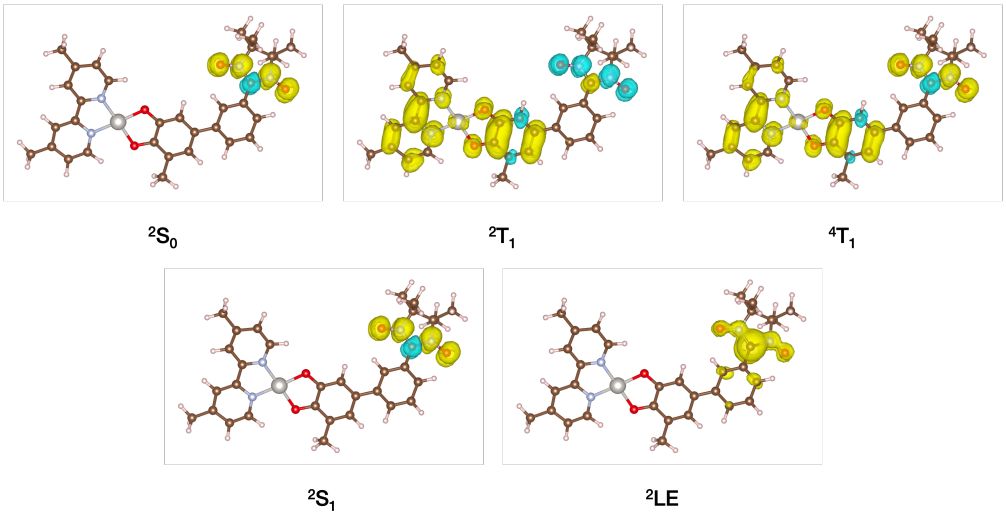

Figure S14: XMS-CASPT2 spin density for bpy-Pt-CAT-*m*Ph-NN (Isosurface value = 0.002).

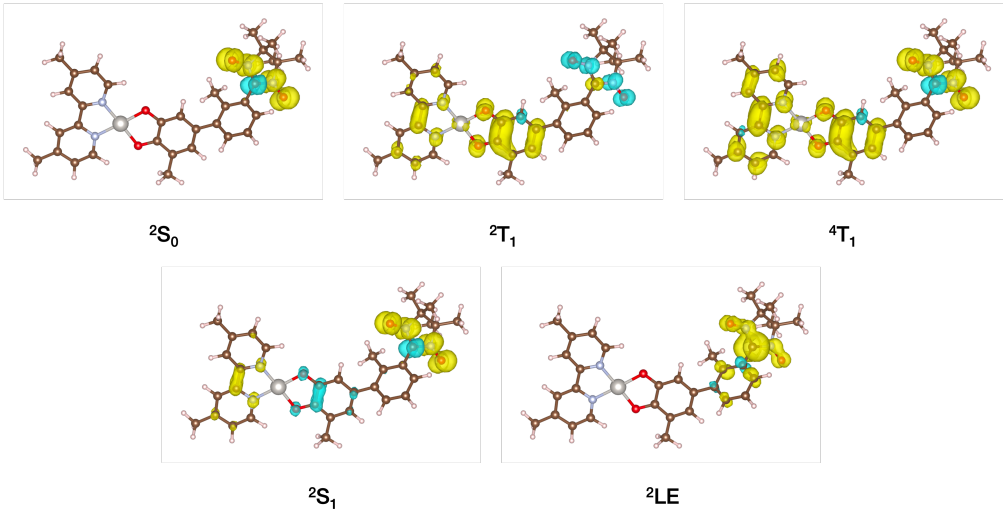

Figure S15: XMS-CASPT2 spin density for bpy-Pt-CAT-2Me-NN (Isosurface value = 0.002).

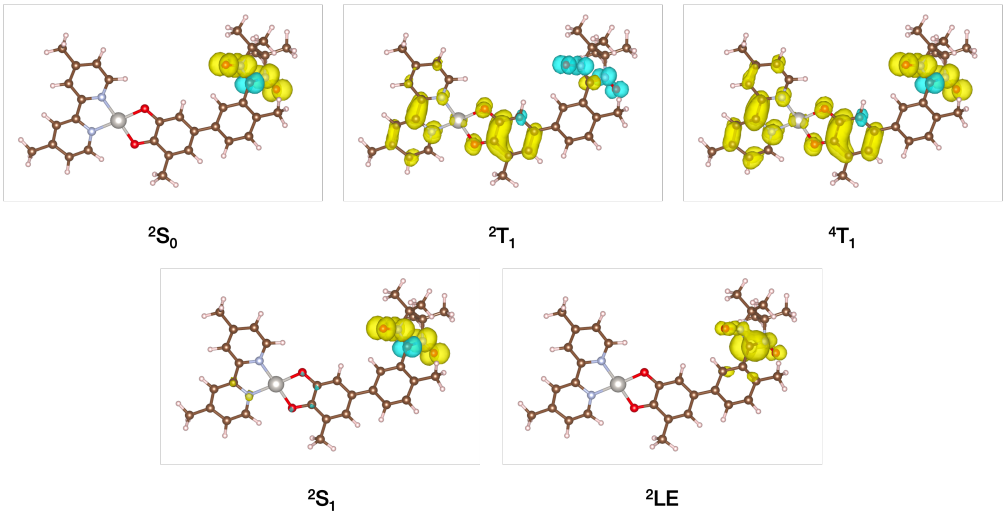

Figure S16: XMS-CASPT2 spin density for bpy-Pt-CAT-4Me-NN (Isosurface value = 0.002).

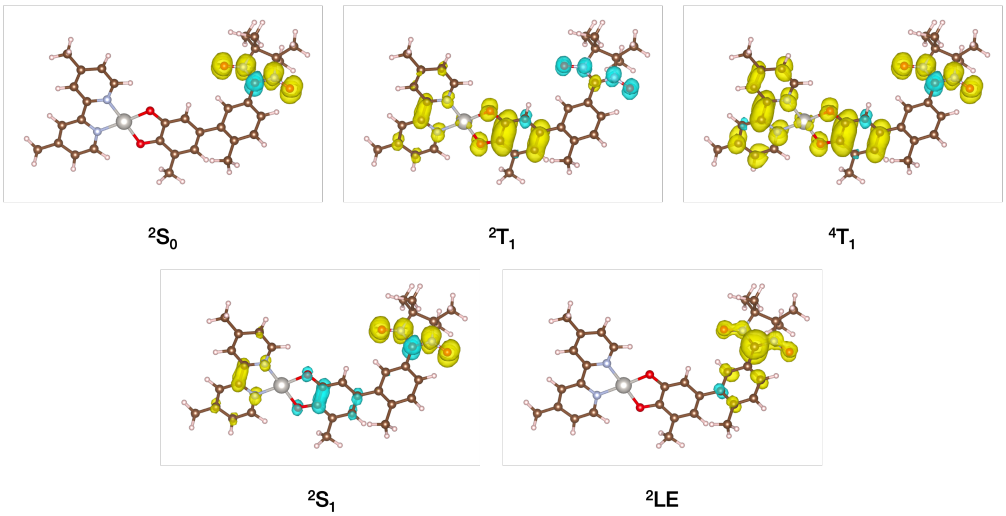

Figure S17: XMS-CASPT2 spin density for bpy-Pt-CAT-6Me-NN (Isosurface value = 0.002).

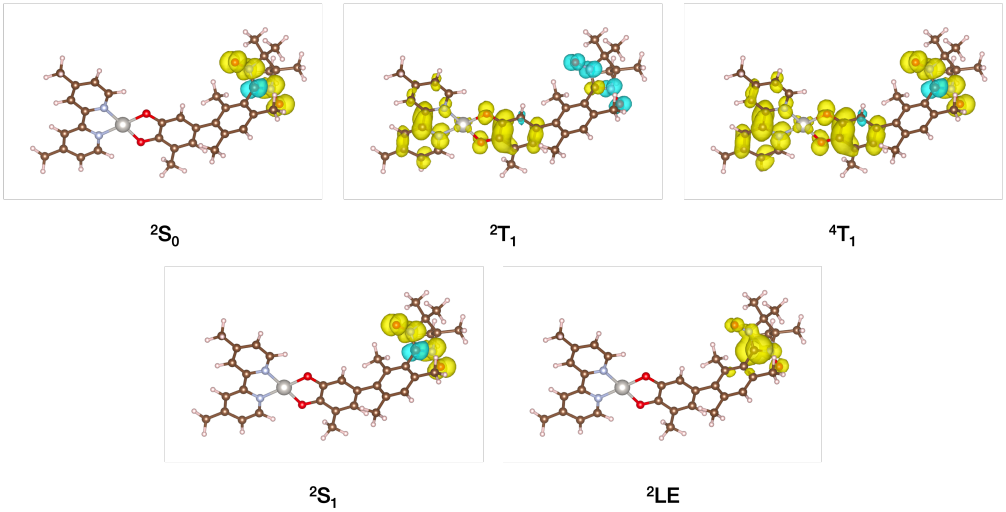

Figure S18: XMS-CASPT2 spin density for bpy-Pt-CAT-246Me-NN (Isosurface value = 0.002).

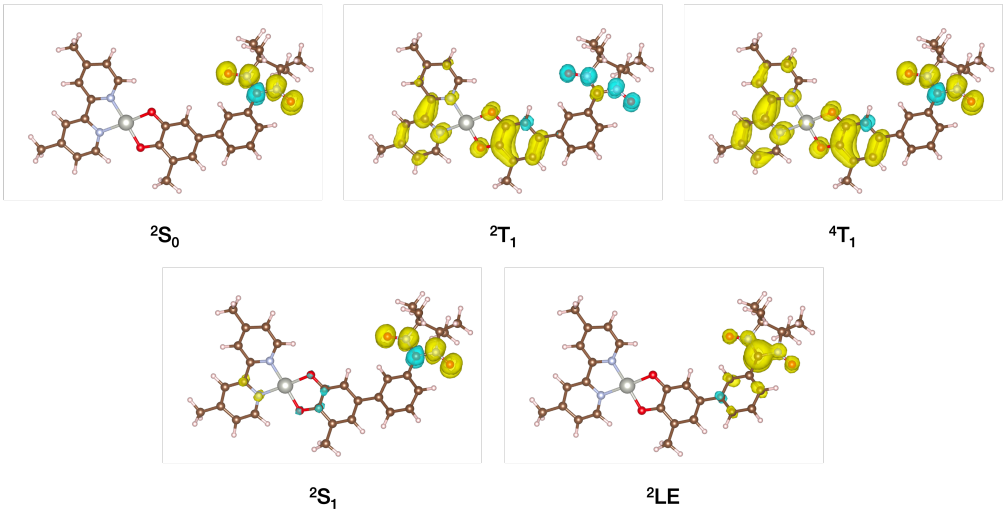

Figure S19: XMS-CASPT2 spin density for bpy-Pd-CAT-*m*Ph-NN (Isosurface value = 0.002).

7 XMS-CASPT2 calculations for bpy-M-NoRadical molecules

Since the radical does not directly participate in the charge-transfer states of bpy-M-CAT-Linker-NN, it can be inferred that the properties are similar even for the molecule with the radical omitted. For comparison, we performed XMS-CASPT2 calculations on bpy-M-NoRadical (Fig. S20), in which the radical and the linker were replaced with the methyl group. The calculation settings were identical to those used in the calculations described in the main text. However, since the radical is not included, the state averaging in the CASSCF was targeted to eight singlet states and three triplet states, and the active space consisted of 12 electrons in 12 orbitals (Fig. S21,S22).

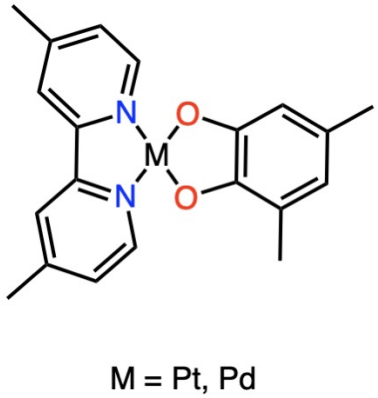

Figure S20: The chemical structure of bpy-M-NoRadical.

Table S4: Excitation energies of bpy-M-NoRadical molecules calculated using XMS-CASPT2. Both structures were optimized for their ground states.

	T_1 / cm^{-1}	S_1 / cm^{-1}
bpy-Pt-NoRadical	16599	17177
bpy-Pd-NoRadical	11882	12033

In bpy-Pt-NoRadical, the calculation indicated the presence of a donor-acceptor charge-transfer excited state at an energy comparable to that of the analogous connected systems; however, the excitation energy of the Pd complex was underestimated relative to the experimental value. This behavior is consistent with the results obtained for bpy-M-CAT-Linker-NN described in the main text, leading us to conclude that a systematic underestimation error exists for the Pd complex.

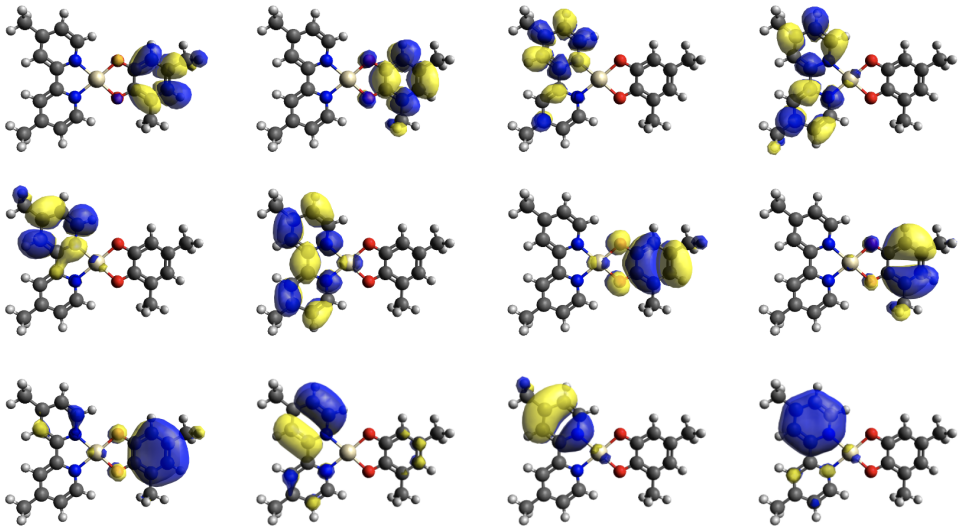

Figure S21: Illustration of CASSCF converged natural orbitals of bpy-Pt-NoRadical with 12 orbitals and 12 electrons. The isosurface value was set to 0.02.

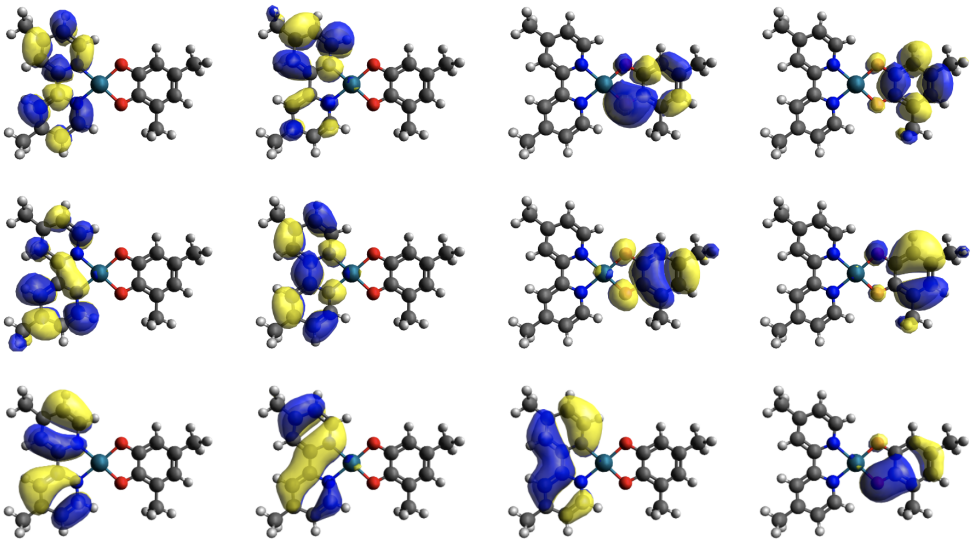

Figure S22: Illustration of CASSCF converged natural orbitals of bpy-Pd-NoRadical with 12 orbitals and 12 electrons. The isosurface value was set to 0.02.

Table S5: CI Vector weights for the T_1 and S_1 states calculated using XMS-CASPT2 theory. The CI vectors obtained from the preceding CASSCF calculations were rotated to diagnalize the effective Hamiltonian in the XMS-CASPT2 framework to correspond with the XMS-CASPT2 wavefunctions. The major Slater determinants contributing to each state are listed. The Slater determinants for both states represent the LUMO localized on the acceptor and HOMO localized on the donor.

	S_0	T_1	S_1	
	$\|02\rangle$	$\|\alpha\alpha\rangle$	$\|\alpha\beta\rangle$	$\|\beta\alpha\rangle$
bpy-Pt-NoRadical	0.78278	0.77498	0.37678	0.37678
bpy-Pd-NoRadical	0.83501	0.83759	0.40318	0.40318

8 Active spaces of PhNN and its derivatives

In this section, we illustrate the orbitals in the active spaces employed in the CASPT2 calculations for PhNN and its derivatives. All active spaces consist of seven electrons in seven orbitals, comprised of the π orbitals of the radical and the Ph group.

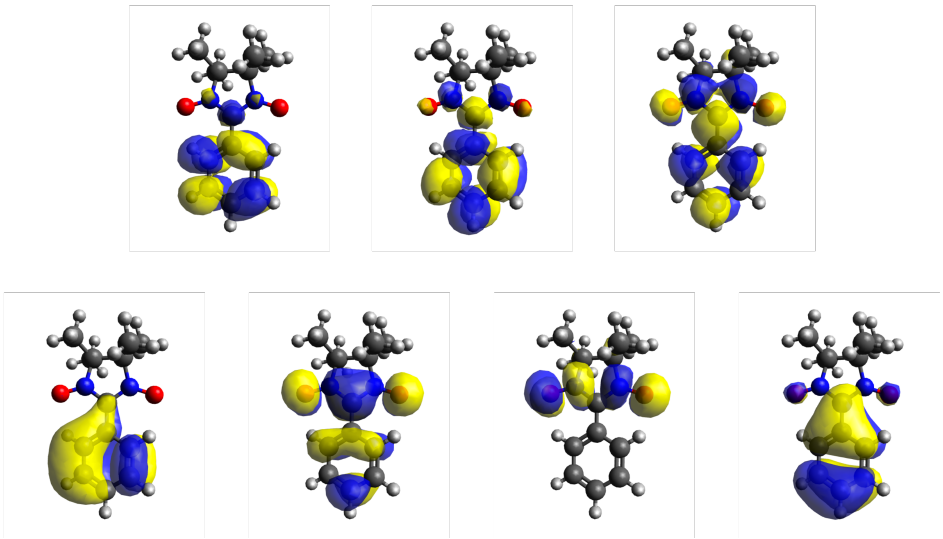

Figure S23: Illustration of CASSCF converged seven natural orbitals of PhNN with seven electrons. The isosurface value was set to 0.02.

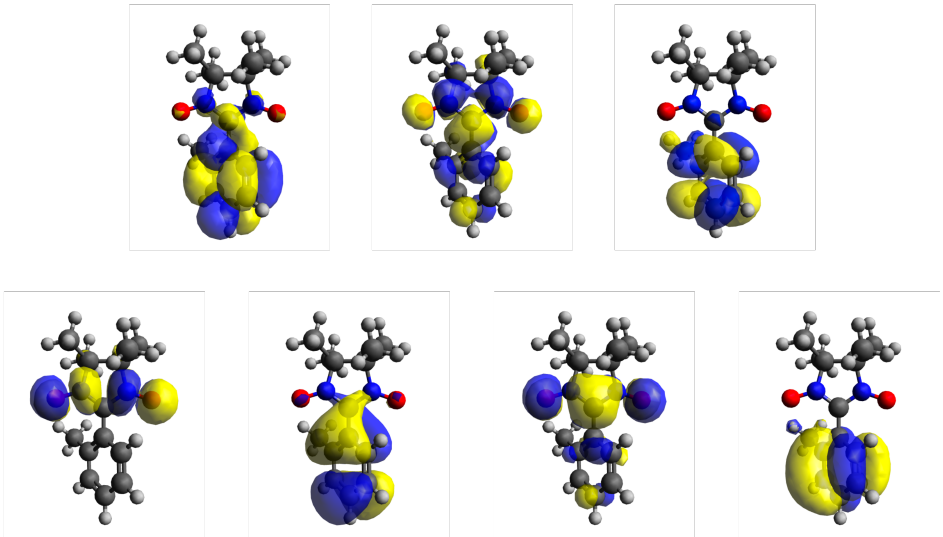

Figure S24: Illustration of CASSCF converged seven natural orbitals of PhNN-2Me with seven electrons. The isosurface value was set to 0.02.

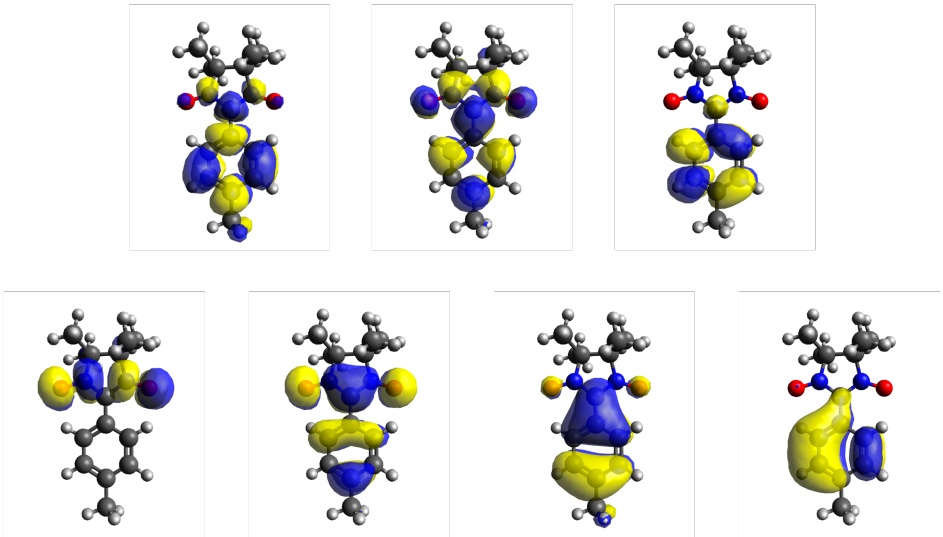

Figure S25: Illustration of CASSCF converged seven natural orbitals of PhNN-6Me with seven electrons. The isosurface value was set to 0.02.

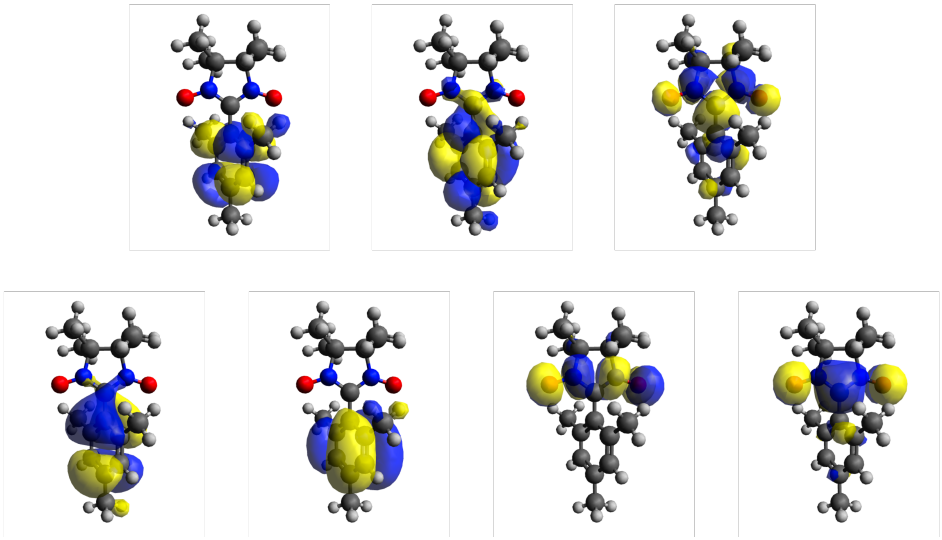

Figure S26: Illustration of CASSCF converged seven natural orbitals of PhNN-2,4,6Me with seven electrons. The isosurface value was set to 0.02.

9 The order of initial guess orbitals in DMRG-CASSCF calculations

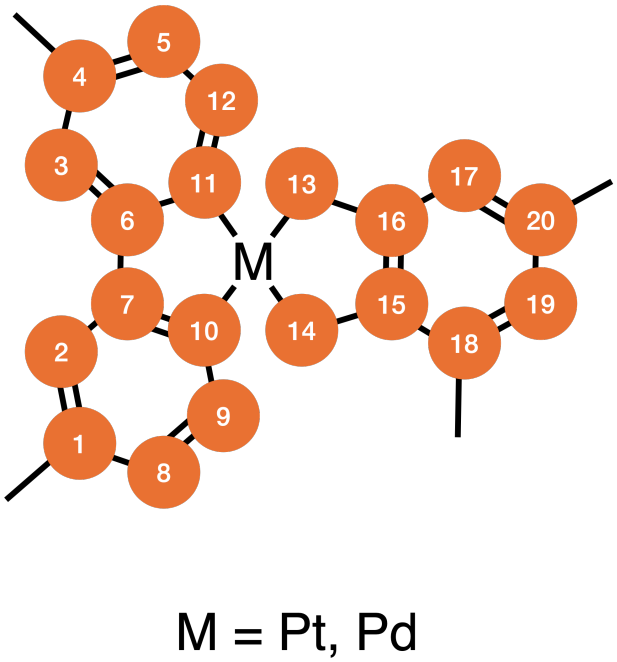

Figure S27: The order of localized orbital sites used in DMRG-CASSCF calculations for bpy-Pt-NoRadical and bpy-Pd-NoRadical.

10 DMRG convergence with respect to bond dimension

Table S6: Convergence of computed wavefunction energies for bpy-Pt-NoRadical and bpy-Pd-NoRadical as a function of bond dimension (M). Note that DMRG-CASSCF calculations did not meet convergence criteria within 150 cycles for M = 128 and 256.

	E[M = 128*] / hartree	E[M = 256*] / hartree	E[M = 512] / hartree	E[M = 1024] / hartree
bpy-Pt-NoRadical	-15998.4059885225	-15998.4069557392	-15998.4071488857	-15998.4071748683
bpy-Pd-NoRadical	-5860.75240873231	-5860.75381470898	-5860.75410709578	-5860.75414018296

The wavefunction energies obtained from the DMRG-CASSCF calculations, as discussed in Section 3.3, are summarized in Table S6. The change in wavefunction energy with increasing bond dimension remains larger than the order of the D-tensor, even when comparing M = 512 and M = 1024. However, as the D-tensor is determined via Eq. (5) (Section 2 of the main text) using the density matrix derived from the DMRG wavefunction (Eq. (7)) and the spin-spin integrals (Eq. (6)), the absolute energy difference in the DMRG wavefunction itself is not crucial. Instead, the accuracy of the density matrix is more critical for the precision of the D-tensor. Given that the DMRG-CASSCF calculations satisfy the convergence criteria at M = 512 and 1024, we conclude that the computational accuracy is sufficient.

11 Derivation of SOC transition matrix elements between quartet and doublet states

In this section, we derive the transition matrix elements for the SOC Hamiltonian used in Section 3.4 of the main text. The notation and derivation essentially follow the work of Ganyushin and Neese (Ref[S3]). To proceed with deriving the transition matrix elements, it is first necessary to establish the form of the SOC Hamiltonian. We begin with the spin-orbit mean-field (SOMF) approach proposed by Hess et al., in which the SOC operator is expressed using a quasi-one-particle operator, as shown in Eq. 1.

$$\hat{H}_{\mathrm{SOMF}} = \sum_i \hat{\mathbf{z}}(i)\hat{\mathbf{s}}(i) \tag{1}$$

It is helpful to represent the operator in the form of the spherical tensor to obtain the expression for the matrix elements. By representing the SOMF operator with the spherical tensor formalism, Eq. 1 can be rewritten as shown in Eq. 2.

$$\hat{H}_{\mathrm{SOMF}} = \sum_{m=0,\pm1} (-1)^m \sum_i \hat{z}_{-m}(i)\hat{s}_m(i). \tag{2}$$

Using the Wigner-Eckart theorem, the matrix elements of the SOMF operator for electronic wavefunctions that consider spin sublevels can be represented by extracting information about sublevels within the Clebsch-Gordan coefficients ($\langle S'M'1m|SM\rangle$) (Eq. 3).

$$\begin{aligned} &\left\langle \Psi_I^{SM} \middle| \sum_{m=0,\pm1} (-1)^m \sum_i \hat{z}_{-m}(i)\hat{s}_m(i) \middle| \Psi_J^{S'M'} \right\rangle \\ &= \frac{1}{\sqrt{2S+1}} \langle S'M'1m|SM\rangle \underbrace{\left\langle \Psi_I^{S} \middle\| \sum_i \hat{z}_{-m}(i)\hat{s}(i) \middle\| \Psi_J^{S'} \right\rangle}_{Y_{IJ}^{SS'}(-m)} \end{aligned} \tag{3}$$

In Eq. 3, Ψ_I^{SM} represents the electronic wavefunction, in which I denotes the state, S is the total spin

quantum number, and M is the spin magnetic quantum number. $Y_{IJ}^{SS'}(-m)$ is the reduced matrix element, which does not include the effects of quartet and doublet sublevels. From Eq. 3, it can be seen that the matrix elements are determined by the Clebsch-Gordan coefficients and the reduced matrix elements. The calculated values for each spin sublevel are listed in Table S7. Although Y_{QD} depends on m, for simplicity, the elements of Y_{QD} for all m values are assumed to be the same. Due to the assumption mentioned above, the spatial part of the molecular wavefunction with respect to the SOMF operator is isotropic. By squaring and taking the spatial average, the matrix elements for the SOC operator that appear in the main text can be derived. Although the derivation of SOC matrix elements presented here is based on the assumption of a SOMF Hamiltonian, it is fully applicable to SOC matrix elements computed using the FNSSO approximation. This is because both approaches reduce the two-electron SOC contributions to an effective one-electron operator, allowing the same formal derivation to be applied without any additional complications.

Table S7: Transition matrix elements of quartet - doublet intersystem crossing via SOMF Hamiltonian.

$\left\langle \mathrm{Q}^{\pm 3/2} \vert \hat{H}_{\mathrm{SOMF}} \vert \mathrm{D}^{\pm 1/2} \right\rangle$	$\left\langle \mathrm{Q}^{\pm 1/2} \vert \hat{H}_{\mathrm{SOMF}} \vert \mathrm{D}^{\pm 1/2} \right\rangle$	$\left\langle \mathrm{Q}^{\mp 1/2} \vert \hat{H}_{\mathrm{SOMF}} \vert \mathrm{D}^{\pm 1/2} \right\rangle$	$\left\langle \mathrm{Q}^{\mp 3/2} \vert \hat{H}_{\mathrm{SOMF}} \vert \mathrm{D}^{\pm 1/2} \right\rangle$
$Y_{QD}(-1)/2$	$Y_{QD}(0)/\sqrt{6}$	$Y_{QD}(1)/\sqrt{12}$	0

12 Investigation of the multi-reference character of PhNN using mutual information

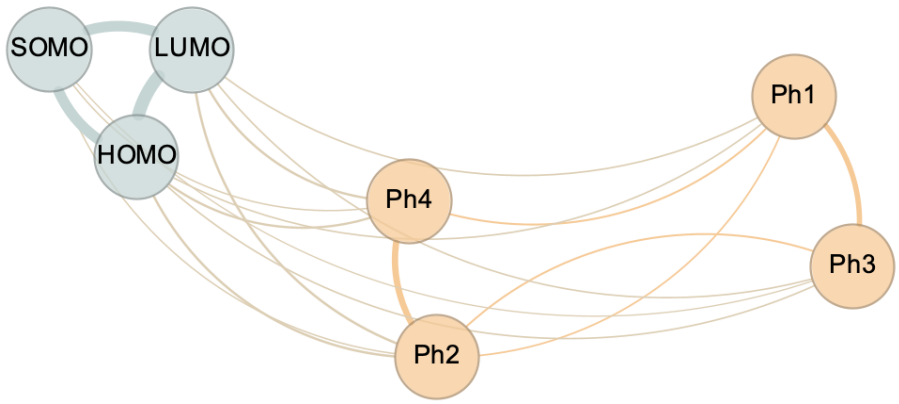

Figure S28: Quantum orbital entanglement (mutual information) maps between the natural active space orbitals of the ^{4}LE state of PhNN. The thickness of the lines gives the magnitude of the mutual information I_pq between the orbitals. Each node in the map denotes a phenyl π orbital (Ph1–Ph4) or a radical π orbital (HOMO, SOMO, LUMO).

Table S8: Mutual information I_{pq} of the ^{4}LE state between the natural active space orbitals of PhNN. The orbitals are visualized in Fig. S29.

	HOMO	SOMO	LUMO	Ph1	Ph2	Ph3	Ph4
HOMO	–	0.287341	0.357856	0.009892	0.035749	0.011053	0.033191
SOMO	0.287341	–	0.286861	–	0.006529	0.001660	0.006474
LUMO	0.357856	0.286861	–	0.011545	0.036853	0.011696	0.034956
Ph1	0.009892	–	0.011545	–	0.014778	0.125185	0.021716
Ph2	0.035749	0.006529	0.036853	0.014778	–	0.021205	0.154740
Ph3	0.011053	0.001660	0.011696	0.125185	0.021205	–	–
Ph4	0.033191	0.006474	0.034956	0.021716	0.154740	–	–

In order to examine the multi-reference character of the PhNN molecule in greater detail, we computed the mutual information within the active space to quantify the degree of orbital entanglement.[S4] Mutual information I_{pq}, which quantifies the quantum entanglement between two orbitals, is defined by the following equation.

$$I_{pq} = s_p + s_q - s_{pq} \tag{4}$$

In this equation, the single-orbital (one-electron) entropies for orbitals s_p and s_q, for orbitals p and q, respectively, and the two-orbital (two-electron) entropy s_{pq} for orbitals p and q are given by:

$$s_p = -\sum_n \rho_{p,n} \ln(\rho_{p,n}) \tag{5}$$

$$s_{pq} = -\sum_{n,m} \rho_{pq,n,m} \ln\left(\rho_{pq,n,m}\right) \tag{6}$$

where $\rho_{p,n}$ and $\rho_{pq,n,m}$ are elements of the single-orbital and two-orbital reduced density matrices, respectively. Typically, the single-orbital entropy s_p ranges from 0 to $\ln 4$ for systems in which each orbital can accommodate up to two electrons (accounting for spin). A value near 0 indicates that the orbital is almost empty or fully occupied (and thus has little uncertainty in its occupancy), whereas the value close to $\ln 4$ suggests a more even distribution of occupancy. The two-orbital entropy s_{pq} captures the combined occupancy distribution of orbitals p and q. Physically, the mutual information I_{pq} measures the degree of correlation between orbitals p and q. By definition, $s_p + s_q \geq s_{pq}$, which guarantees $I_{pq} = s_p + s_q - s_{pq}$ is nonnegative. When I_{pq} is zero, it indicates that the two orbitals are uncorrelated and independent. In contrast, when the value of I_pq is near the maximum value, $2\ln 4$, it reflects a high degree of interdependence between the occupation states of orbitals p and q, signifying strong electron correlation effects in the system. Because mutual information directly quantifies the electron correlation between orbital pairs, it has been demonstrated to reliably reflect the presence of static correlation effects. In systems where a single-reference description is insufficient, strong orbital entanglement—manifested as high mutual information—signals significant contributions from multiple electronic configurations. Thus, elevated values of I_{pq} serve as a robust indicator of multi-reference character, supporting the need for advanced correlated methods to accurately capture the system's electronic structure.[S5,S6] In Ref.[S6], it is stated that orbital pairs with mutual information of approximately 0.1 or higher exhibit significant static electron correlation.

For the calculations, we computed the mutual information for each orbital pair employing the same active space of 7 electrons in 7 orbitals as used in the CASPT2 calculations. All other

computational conditions, aside from the DMRG algorithm, were maintained identical to those used in the CASPT2 calculations. The bond dimension was set to 2048. We selected natural orbitals for calculating the mutual information, and the orbitals within the active space with their labels are visualized in Fig. S29. Mutual information of the ^{4}LE state for each orbital pair is presented in Fig. S28 and Table S8. The network graph was drawn using the network visualization software Gephi.[S7]

The mutual information between orbitals in the radical region is around 0.3, indicating strong electron correlation of the ^{4}LE state. Additionally, orbital pairs between the occupied and unoccupied portions of the phenyl ring each exhibit values exceeding 0.1. Combining these results with the T_1-diagnostic values, we concluded that it is advantageous to cross-validate the computed energies using multi-reference methods such as CASPT2.

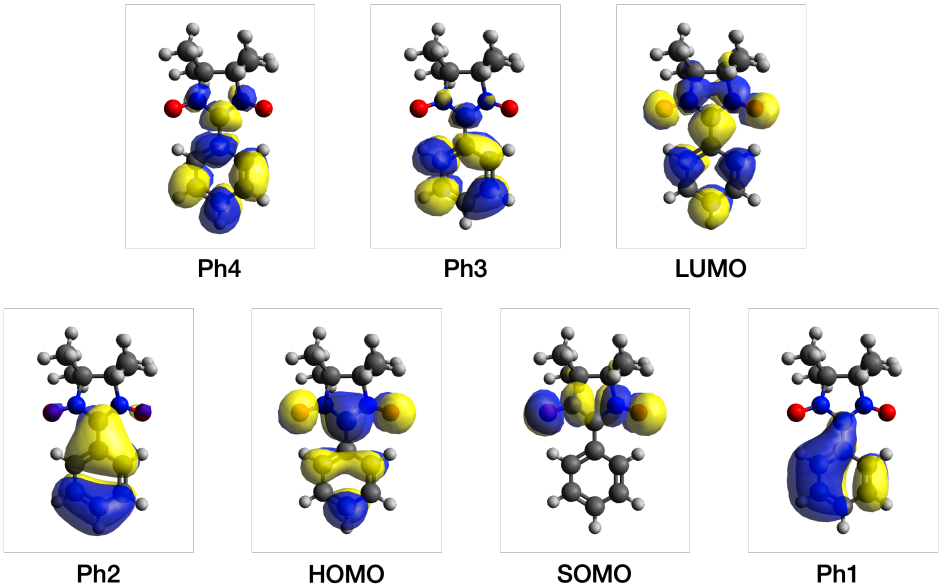

Figure S29: Natural active space orbitals of PhNN for the DMRG-CASSCF calculation.

13 Coupled cluster calculations of PhNN

We attempted to reproduce calculations at the CCSD(T) level to obtain excited-state information for PhNN. To validate and compare our results, we performed a series of calculations using the domain-based local pair natural orbital coupled cluster theory with single, double, and perturbative triple excitations (DLPNO-CCSD(T)).[S8–S12] This method is renowned for its ability to accurately capture electron correlation while significantly reducing computational costs by partitioning the electron correlation into localized electron-pair domains using compact pair natural orbitals. Such efficiency renders it particularly suitable for larger or more complex molecular systems, as it closely approximates the full CCSD(T) treatment without compromising reliability.[S13]

DLPNO-CCSD(T) calculations for the ground state of open-shell systems were performed using an unrestricted Hartree-Fock (UHF) reference wavefunction. The structure was optimized at the DFT BP86/def2-TZVP level of theory, as noted in the main text. The correlation-consistent (cc-pVnZ, n=D,T,Q,5) basis sets[S14,S15] were employed, and the corresponding cc-pVnZ/C auxiliary basis sets[S16] were utilized to enable the RI approximation. All calculations were carried out using the ORCA 6.0 software package.[S17,S18]

Table S9: DLPNO-CCSD(T) energy comparison of PhNN for each basis set. The values in parentheses are T_1-diagnostic.

Basis set	E[D] (Eh)	E[Q] (Eh)	ΔE(D-Q) (cm^{-1})
cc-pVDZ	-763.3909090 (0.0170)	-763.3909532 (0.0197)	17790
cc-pVTZ	-764.1410461 (0.0169)	-764.0545741 (0.0200)	17896
cc-pVQZ	-764.3644659 (0.0167)	-764.2758768 (0.0197)	19463
cc-pV5Z	-764.4336852 (0.0165)	-764.3441240 (0.0202)	19654
CBS (Q,5)*	-764.4975650	-764.4072783	19816

*Two-point extrapolation with the cc-pVQZ and cc-pV5Z basis sets, $z = 6.30$ and $y = 3.0$.

Table S9 represents the DLPNO-CCSD(T) results for PhNN. Note that the doublet (D) and quartet (Q) energies were computed separately, and their difference was used to determine the lowest quartet excitation energy. The calculations reveal that this lowest quartet state lies in the range of approximately 18000–20000 cm^{-1}, placing it in close proximity to the CT states of bpy-M-CAT-Linker-NN. A slight upward trend in the excitation energy is observed as the basis set

size increases. In our recalculations, we reproduced an excitation energy comparable to that reported in the preceding study mentioned in the main text,[S19] and the T_1-diagnostic values were approximately 0.02.

In addition, to gain further insights into the excited state properties of PhNN, we computed the lowest doublet excited state using the back-transformed pair natural orbital similarity transformed equation of motion coupled cluster with single and double excitations (bt-PNO-STEOM-CCSD) method.[S20] In this approach, the computationally expensive ground-state coupled cluster amplitudes are first obtained using the DLPNO-CCSD method and then back-transformed to a canonical basis. A second similarity transformation is subsequently applied, which decouples the single excitations from the doubles, thereby enabling the excitation energies to be determined by diagonalizing the transformed Hamiltonian in the single excitation space only. According to the benchmark in Ref[S20], this method achieves nearly identical performance to canonical STEOM-CCSD for both singlet and triplet excited states while offering significant computational efficiency gains.

Excited-state calculations were performed at the bt-PNO-STEOM-CCSD level of theory using the ORCA 6.0. The UHF reference wavefunction was employed, and the cc-pVDZ basis set was used. Basis sets larger than cc-pVTZ were not used due to computational memory issues. The corresponding cc-pVDZ/C auxiliary basis set was applied, while the def2/J auxiliary basis set[S21] was used for the Coulomb fitting.

Our calculation for the lowest doublet excited state using the bt-PNO-STEOM-CCSD method yielded an excitation energy of 12661 cm^{-1}. Even after accounting for solvent effects compared to the gas phase, this value differs substantially from the experimental value of 15699 cm^{-1} in hexane.[S22] Therefore, it remains possible that the excitation energy of the ^{4}LE state is also underestimated even at the CCSD level.

References

(S1) Momma, K.; Izumi, F. VESTA 3 for Three-Dimensional Visualization of Crystal, Volumetric and Morphology Data. J. Appl. Crystallogr. **2011**, 44, 1272–1276.

(S2) Hanwell, M. D.; Curtis, D. E.; Lonie, D. C.; Vandermeersch, T.; Zurek, E.; Hutchison, G. R. Avogadro: An Advanced Semantic Chemical Editor, Visualization, and Analysis Platform. J. Cheminf. **2012**, 4, 17.

(S3) Ganyushin, D.; Neese, F. First-Principles Calculations of Zero-Field Splitting Parameters. J. Chem. Phys. **2006**, 125, 024103.

(S4) Rissler, J.; Noack, R. M.; White, S. R. Measuring Orbital Interaction Using Quantum Information Theory. Chem. Phys. **2006**, 323, 519–531.

(S5) Boguslawski, K.; Tecmer, P.; Legeza, Ö.; Reiher, M. Entanglement Measures for Single- and Multireference Correlation Effects. J. Phys. Chem. Lett. **2012**, 3, 3129–3135.

(S6) Boguslawski, K.; Réal, F.; Tecmer, P.; Duperrouzel, C.; Gomes, A. S. P.; Legeza, Ö.; Ayers, P. W.; Vallet, V. On the Multi-Reference Nature of Plutonium Oxides: PuO22+, PuO2, PuO3 and PuO2(OH)2. Phys. Chem. Chem. Phys. **2017**, 19, 4317–4329.

(S7) Bastian, M.; Heymann, S.; Jacomy, M. Gephi: An Open Source Software for Exploring and Manipulating Networks. 2009; `http://www.aaai.org/ocs/index.php/ICWSM/09/paper/view/154`.

(S8) Neese, F.; Hansen, A.; Liakos, D. G. Efficient and Accurate Approximations to the Local Coupled Cluster Singles Doubles Method Using a Truncated Pair Natural Orbital Basis. J. Chem. Phys. **2009**, 131, 064103.

(S9) Neese, F.; Wennmohs, F.; Hansen, A. Efficient and Accurate Local Approximations to Coupled-Electron Pair Approaches: An Attempt to Revive the Pair Natural Orbital Method. J. Chem. Phys. **2009**, 130, 114108.

(S10) Riplinger, C.; Pinski, P.; Becker, U.; Valeev, E. F.; Neese, F. Sparse Maps—A Systematic Infrastructure for Reduced-Scaling Electronic Structure Methods. II. Linear Scaling Domain Based Pair Natural Orbital Coupled Cluster Theory. J. Chem. Phys. **2016**, 144, 024109.

(S11) Saitow, M.; Becker, U.; Riplinger, C.; Valeev, E. F.; Neese, F. A New Near-Linear Scaling, Efficient and Accurate, Open-Shell Domain-Based Local Pair Natural Orbital Coupled Cluster Singles and Doubles Theory. J. Chem. Phys. **2017**, 146, 164105.

(S12) Guo, Y.; Riplinger, C.; Becker, U.; Liakos, D. G.; Minenkov, Y.; Cavallo, L.; Neese, F. Communication: An Improved Linear Scaling Perturbative Triples Correction for the Domain Based Local Pair-Natural Orbital Based Singles and Doubles Coupled Cluster Method [DLPNO-CCSD(T)]. J. Chem. Phys. **2018**, 148, 011101.

(S13) Liakos, D. G.; Guo, Y.; Neese, F. Comprehensive Benchmark Results for the Domain Based Local Pair Natural Orbital Coupled Cluster Method (DLPNO-CCSD(T)) for Closed- and Open-Shell Systems. J. Phys. Chem. A **2020**, 124, 90–100.

(S14) Dunning, T. H., Jr. Gaussian Basis Sets for Use in Correlated Molecular Calculations. I. The Atoms Boron through Neon and Hydrogen. J. Chem. Phys. **1989**, 90, 1007–1023.

(S15) Kendall, R. A.; Dunning, T. H., Jr.; Harrison, R. J. Electron Affinities of the First-row Atoms Revisited. Systematic Basis Sets and Wave Functions. J. Chem. Phys. **1992**, 96, 6796–6806.

(S16) Weigend, F.; Köhn, A.; Hättig, C. Efficient Use of the Correlation Consistent Basis Sets in Resolution of the Identity MP2 Calculations. J. Chem. Phys. **2002**, 116, 3175–3183.

(S17) Neese, F. Software Update: The ORCA Program System—Version 5.0. WIREs Comput. Mol. Sci. **2022**, 12, e1606.

(S18) Neese, F. The SHARK Integral Generation and Digestion System. J. Comp. Chem. **2023**, 44, 381–396.

(S19) Kirk, M. L.; Shultz, D. A.; Chen, J.; Hewitt, P.; Daley, D.; Paudel, S.; van der Est, A. Metal Ion Control of Photoinduced Electron Spin Polarization in Electronic Ground States. J. Am. Chem. Soc. **2021**, 143, 10519–10523.

(S20) Dutta, A. K.; Nooijen, M.; Neese, F.; Izsák, R. Exploring the Accuracy of a Low Scaling Similarity Transformed Equation of Motion Method for Vertical Excitation Energies. J. Chem. Theory Comput. **2018**, 14, 72–91.

(S21) Weigend, F. Accurate Coulomb-fitting Basis Sets for H to Rn. Phys. Chem. Chem. Phys. **2006**, 8, 1057.

(S22) Ullman, E. F.; Osiecki, J. H.; Boocock, D. G. B.; Darcy, R. Stable Free Radicals. X. Nitronyl Nitroxide Monoradicals and Biradicals as Possible Small Molecule Spin Labels. J. Am. Chem. Soc. **1972**, 94, 7049–7059.